



ORIGINAL ARTICLE

Regio- and stereoselectivity of the 1,3-dipolar cycloaddition of azomethine ylides to (*E*)-3-(2-oxo-2-(pyren-1-yl)ethylidene)indolin-2-ones: A combined experimental and theoretical study



Essam M. Hussein^{a,b,*}, Ziad Moussa^c, Uttam Pal^d, Reem I. Alsantali^e,
Abdullah Y.A. Alzahrani^f, Rami J. Obaid^a, Fawaz M. Alzahrani^{a,g},
Munirah M. Al-Rooqi^a, Meshari A. Alsharif^a, Nizar El Guesmi^{a,h},
Rabab S. Jassasⁱ, M. Shaheer Malik^a, Hatem M. Altass^a, Samir K. Pal^j,
Tanusri Saha Dasgupta^k, Saleh A. Ahmed^{a,b,*}

^a Department of Chemistry, Faculty of Applied Science, Umm Al-Qura University, 21955 Makkah, Saudi Arabia

^b Department of Chemistry, Faculty of Science, Assiut University, 71516 Assiut, Egypt

^c Department of Chemistry, College of Science, United Arab Emirates University, P.O. Box 15551, Al Ain, United Arab Emirates

^d Technical Research Centre, S.N.Bose National Centre for Basic Sciences, Block JD, Sector III, Salt Lake, Kolkata 700 106, India

^e Department of Pharmaceutical Chemistry, College of Pharmacy, Taif University, P.O.Box 11099, Taif 21944, Saudi Arabia

^f Department of Chemistry, Faculty of Science and Arts, King Khalid University, Mohail, Assir, Saudi Arabia

^g Research Laboratories Unit, Faculty of Applied Science, Umm Al-Qura University, 21955 Makkah, Saudi Arabia

^h Département de chimie, Faculté des Sciences de Monastir, Avenue de l'Environnement, 5019 Monastir, Tunisia

ⁱ Department of Chemistry, Jamoum University College, Umm Al-Qura University, 21955 Makkah, Saudi Arabia

^j Department of Chemical, Biological & Macromolecular Sciences, S.N. Bose National Centre for Basic Sciences, JD Block, Sector III, Salt Lake, Kolkata (Calcutta) 700 106, India

^k Department of Condensed Matter Physics and Material Sciences, S.N.Bose, National Centre for Basic Sciences, Block JD, Sector III, Salt Lake, Kolkata 700 106, India

Received 1 February 2022; accepted 23 March 2022

Available online 29 March 2022

Abbreviations: 1, 1,3-dipolar cycloaddition; 2, azomethine ylides; 3, stereoselectivity; 4, regioselectivity; 5, DFT-theory

* Corresponding authors at: Department of Chemistry, Faculty of Applied Science, Umm Al-Qura University, 21955 Makkah, Saudi Arabia.

E-mail addresses: amhfarghaly@uqu.edu.sa, essam.hussein78@yahoo.com (E.M. Hussein), saahmed@uqu.edu.sa, saleh_63@hotmail.com (S.A. Ahmed).

Peer review under responsibility of King Saud University.



KEYWORDS

Natural product scaffold;
Multicomponent [3 + 2]
cycloaddition;
DFT;
Transition state;
Local reactivity

Abstract Functionalized oxindoles and pyrrolizidines form the central structural framework for numerous natural products with extensive biological and pharmacological applications. The requirement for high regio- and stereoselectivity is the main obstacle in the synthesis of such five-membered heterocycles. Multicomponent cycloaddition reactions often provide an efficient and straightforward approach for the preparation of specific regio- and stereoisomers. In this article, the regio- and stereochemistry of the polar [3 + 2]-cycloaddition (32CA) reaction of azomethine ylides prepared by the reaction of isatin derivatives and L-proline with a series of (*E*)-3-(2-oxo-2-(pyren-1-yl)ethylidene)indolin-2-ones was investigated by experimental and theoretical methods. Among the isatin and (*E*)-3-(2-oxo-2-(pyren-1-yl)ethylidene)indolin-2-one derivatives, a remarkable inversion of regioselectivity was observed in the 32CA reaction of azomethine ylide generated by the reaction of L-proline and 5-chloroisatin or *N*-methyl-5-chloroisatin with (*E*)-5-chloro-3-(2-oxo-2-(pyren-1-yl)ethylidene)indolin-2-one. The regio- and stereochemical assignment of the structures of the cycloaddition products was determined by one- and two-dimensional (1D&2D) homonuclear and heteronuclear correlation nuclear magnetic resonance spectroscopy. The molecular mechanism as well as the regio- and stereoselectivity of the cycloaddition were investigated by means of global and local reactivity indices and a density functional theory (DFT) and explained in detail on the basis of the transition state stabilities of the reactants.

© 2022 The Author(s). Published by Elsevier B.V. on behalf of King Saud University. This is an open access article under the CC BY-NC-ND license (<http://creativecommons.org/licenses/by-nc-nd/4.0/>).

1. Introduction

The [3 + 2]-cycloaddition (32CA) reactions provide an efficient and straightforward approach to the construction of five-membered heterocycles and very often proceed with high regio- and stereoselectivity (Padwa and Pearson, 2002). Therefore, the intermolecular 32CA reaction of unstabilized azomethine ylides with electron deficient olefins serves as a convenient and efficient protocol for the synthesis of highly functionalized heterocycles such as pyrrolidines and pyrrolizidines containing multiple stereogenic centers in a single step (Dondas et al., 2004).

Functionalized oxindoles and pyrrolizidines serve as the central scaffold for several natural products and represent a class of compounds that exhibit significant biological activity (Monlineux, 1987). Spiropyrrolizidine oxindole species have recently attracted considerable attention due to their abundance in many natural products as well as their broad biological and pharmacological applications (Rajeswaran et al., 1999). In addition, the pyrene moiety is one of the most valuable building blocks for the construction of fluorogenic chemosensors (Weng et al., 2012).

In the last decades, the understanding of the mechanism and underlying principles of the polar 32CA process in addition to selectivity has grown through several studies that have investigated the interplay between theoretical and experimental aspects, although it remains a challenge to this day (Merino et al., 2003). Several mechanisms have been proposed to explain the [3 + 2] cycloaddition (32CA) reaction which has experienced a recent resurgence as indicated by the incredible volume of recent studies reported on the subject (Rios-Gutierrez et al., 2019). First, the 32CA reaction consists of an addition reaction between a three-atom component (TAC) and a multiple bond system and the transformation may proceed under metal-free or metal-assisted conditions (Rios-Gutierrez et al., 2019). The former is a neutral species

whose core structure is composed from three nuclei sharing at least 8 electrons. TACs can be geometrically categorized into two types: linear (L-TAC) and bent (B-TAC) geometries. Mechanistically, Huisgen originally proposed that three mechanisms were plausible (i) the positive end of the TAC may react first, and the negative end would then complete the addition; (ii) the negative pole may attack first and then the positive end would complete the addition; or (iii) both charged ends of the dipole may be added concurrently. While mechanisms i and ii proceed via octet 1,2-dipoles and involve zwitterionic intermediate, mechanism iii takes place via sextet 1,3-dipoles and is concerted. Firestone proposed, an alternative stepwise radical mechanism via formation of a diradical intermediate (Rios-Gutierrez et al., 2019). It has been established that the regio- and stereochemistry of 32CA reactions can be controlled either by selecting the appropriate dipole and/or dipolarophile or by controlling the reaction with a catalyst (Yan et al., 2006). Electronic and steric effects are two key factors that can influence the outcome of the regio- and stereoselectivity of such reactions (Bakthadoss and Sivakumar, 2009). Recently, the molecular mechanism and underlying factors affecting regio- and chemoselectivity in 32CA processes have been theoretically investigated using reactivity indices of density functional theory (DFT) (Domingo et al., 2002) and molecular electron density theory (MEDT) (Domingo, 2016).

As a further extension of our ongoing research on 32CA reactions and their utility for the synthesis of novel spiroheterocycles (Hussein and Abdel-Monem, 2011), we now report the results of experimental and theoretical studies on the regio- and stereoselectivity of the 32CA reaction of azomethine ylides (AYs) **3a-c** (generated in situ from isatins **1a-c** and L-proline (**2**) with a series of (*E*)-3-(2-oxo-2-(pyren-1-yl)ethylidene)indolin-2-one derivatives **4a-d**, in order to obtain a series of hitherto unknown new 1'-(1-pyrenoyl)-dispiro[indoline-3,3'-pyrrolizidin-2',3''-indoline]-2,2''-diones and/or 2'-(1-pyrenoyl)-dispiro[indoline-3,3'-pyrrolizidin-1',3''-indoline]-2,2''-diones.

2. Results and discussion

2.1. Synthetic approach

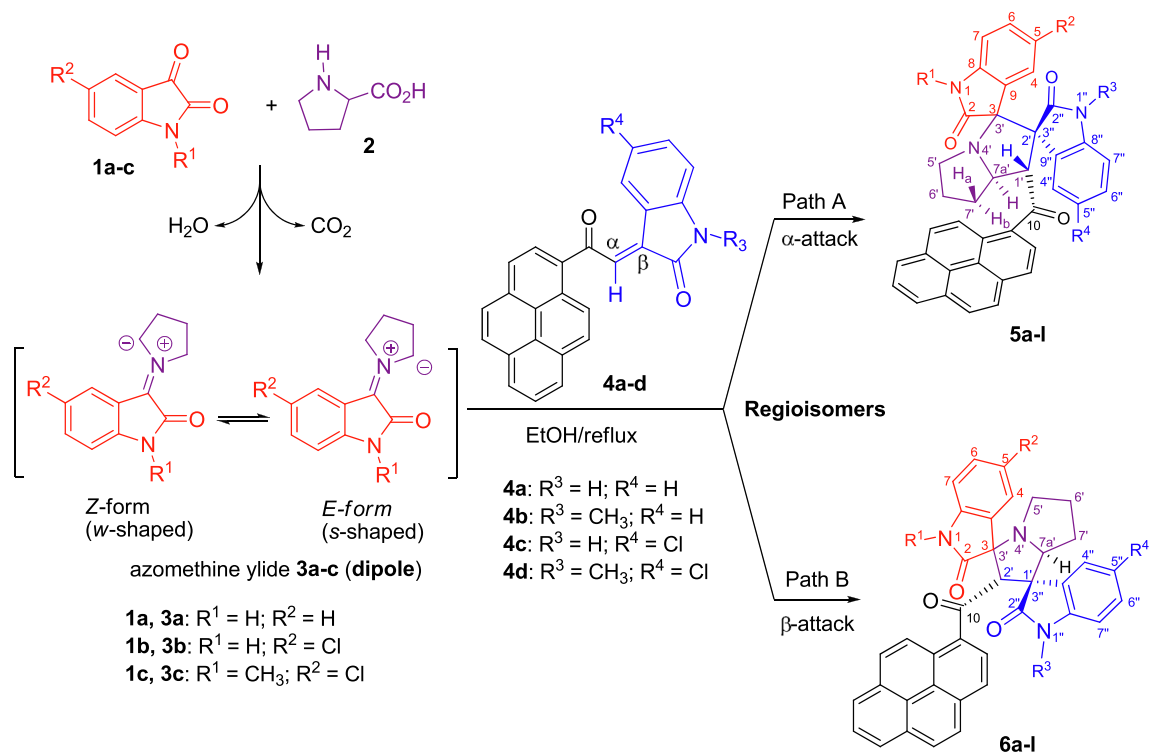
The [3 + 2]-cycloaddition reaction of azomethine ylides (AYs) **3a-c**, generated in situ from the reaction of isatin derivatives **1a-c** and L-proline (**2**) in absolute ethanol under reflux, with (*E*)-3-(2-oxo-2-(pyren-1-yl)ethylidene)indolin-2-one derivatives **4a-d** prepared as dipolarophiles, gave a new series of 1'-(1-pyrenoyl)-dispiro[indoline-3,3'-pyrrolizidine-2',3''-indoline]-2,2''-diones **5a-l** and/or 2'-(1-pyrenoyl)-dispiro[indoline-3,3'-pyrrolizidine-1',3''-indoline]-2,2''-diones **6a-l** (Scheme 1).

The regioisomeric molar ratio was determined by ¹H NMR spectroscopy using C₁-H and C₂-H as distinctive signals for regioisomer **5** and **6**, respectively. The reaction was found to be relatively regioselective and stereospecific at the stereogenic centers. The regiochemistry of the reaction was found to be dependent on the chemical structure of both the dipole and the dipolarophile (Table 1). It can be seen from Table 1 that in most cases, regioisomers **5** were obtained as the major products (Table 1, entries 1–7 & 10–12). Surprisingly, in the case of the 32CA reaction of dipoles **3b** (generated in situ by the reaction of 5-chloroisatin **1b** and L-proline) and **3c** (generated in situ by the reaction of *N*-methyl-5-chloroisatin **1c** and L-proline) with (*E*)-5-chloro-3-(2-oxo-2-(pyren-1-yl)ethylidene)indolin-2-one (**4c**), the regiochemistry was reversed and the cycloadducts **6h** (Table 1, entry 8) and **6i** (Table 1, entry 9) were obtained as the major products. It should be mentioned that the pure regioisomers **5a**, **5b**, **5d**, **5e**, **5j**, **5l** and **6i** were

obtained by recrystallizing the crude reaction mixture from absolute ethanol. Unfortunately, compounds **5c**, **5f**, **5g**, **5h**, **5k** and their corresponding regioisomers could not be separated by either recrystallization or column chromatography because they have similar *R_f* values in different organic solvents.

2.2. Regio- and stereoselectivity

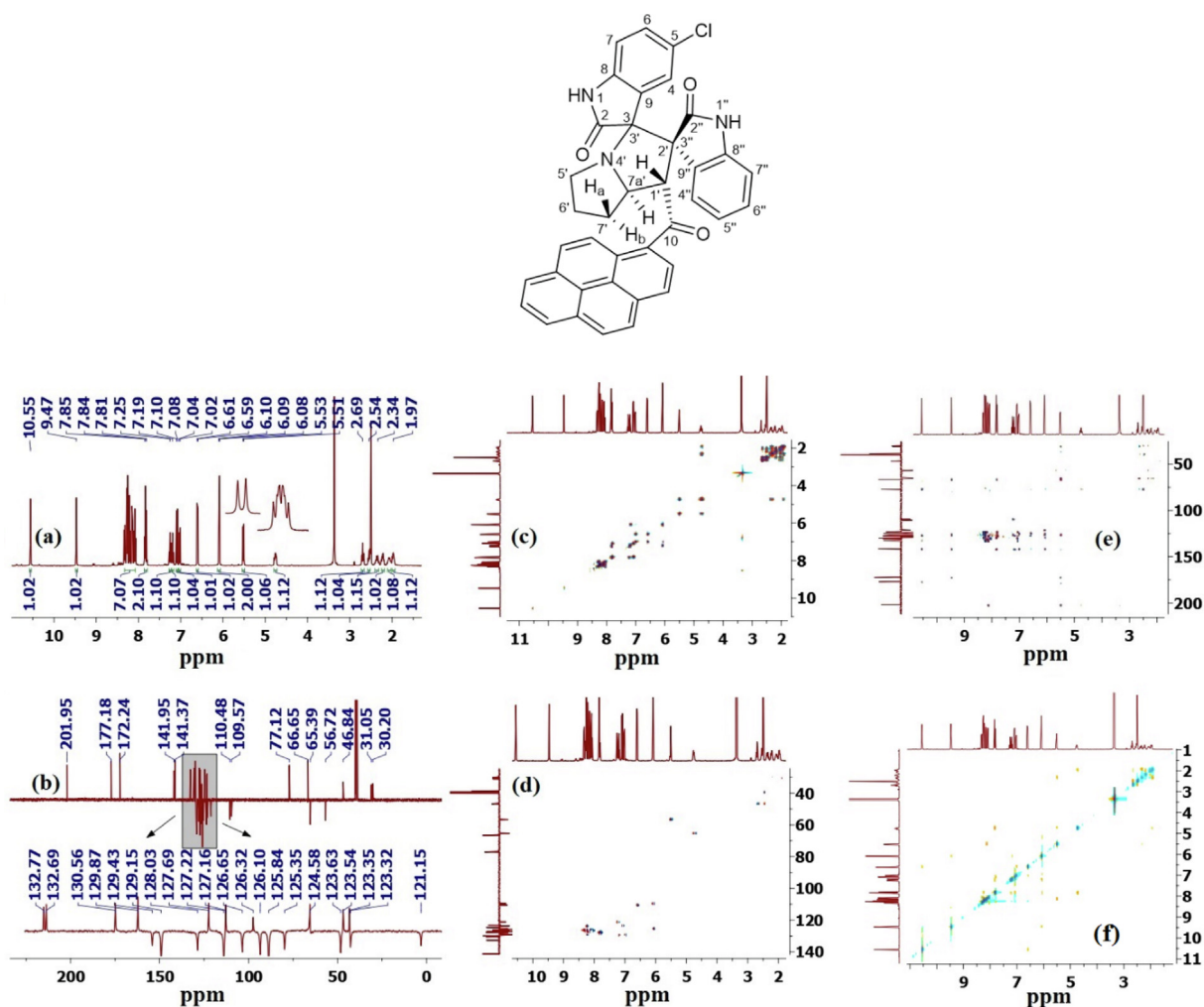
To confirm the chemical structures and regio/stereochemistry of the isolated products for each pair of reacting substrates, we performed multiple one-dimensional (1D) (proton, carbon-13, CRAPT, DEPT-135 NMR) and two-dimensional (2D) homo- and heteronuclear correlation nuclear magnetic resonance spectroscopy measurements (gDQFCOSY, gHSQCAD, HMBCAD, ROESYAD) as well as decoupling experiments on several compounds (Figs. S1–S97). The determination of relative and absolute configuration of organic compounds by various NMR techniques is being frequently used and is a growing field of research as it offers an alternative approach, besides single crystal X-ray crystallography, to determine structure (Bifulco et al., 2007). The NMR technique is useful for non-crystalline samples that resist all type of crystallization into suitable X-ray grade crystals. Therefore, the selection of 5-chloro-1'-(1-pyrenoyl)-dispiro[indoline-3,3'-pyrrolizidine-2',3''-indoline]-2,2''-diones (**5b**) and 5,5''-dichloro-1-methyl-2'-(1-pyrenoyl)-dispiro[indoline-3,3'-pyrrolizidine-1',3''-indoline]-2,2''-diones (**6i**) as representative models for the remaining derivatives in the series, the relevant spectra used for



Scheme 1 Synthesis of 1'-(1-pyrenoyl)-dispiro[indoline-3,3'-pyrrolizidine-2',3''-indoline]-2,2''-diones **5a-l** and 2'-(1-pyrenoyl)-dispiro[indoline-3,3'-pyrrolizidine-1',3''-indoline]-2,2''-diones **6a-l**.

Table 1 32CA reaction of isatins **1a-c** and L-proline (**2**) with dipolarophiles **4a-d**.

Entry	Reactants	Products	Time (h)	Yield ^a (%)	Diastereomeric ratio (%)	Regioisomeric ratio ^b (5:6)
1	1a + 2 + 4a	5a	3.5	97	100	>95:5
2	1b + 2 + 4a	5b	5.5	88	100	>95:5
3	1c + 2 + 4a	5c + 6c	5	86	100	70:30
4	1a + 2 + 4b	5d	3	81	100	>95:5
5	1b + 2 + 4b	5e	5	75	100	>95:5
6	1c + 2 + 4b	5f + 6f	5	71	100	83:17
7	1a + 2 + 4c	5g + 6g	2.5	95	100	59:41
8	1b + 2 + 4c	5h + 6h	5	91	100	27:73
9	1c + 2 + 4c	6i	4.5	78	100	0:100
10	1a + 2 + 4d	5j	2.5	83	100	>95:5
11	1b + 2 + 4d	5k + 6k	4.5	84	100	66:34
12	1c + 2 + 4d	5l	4	67	100	>95:5

^a Combined yield of isolated cycloadducts.^b Determined by ¹H NMR spectroscopy.**Fig. 1** (a) ¹H NMR spectrum of **(5b)**; (b) ¹³C CRAPT-NMR spectrum; (c) ¹H-¹H-COSY-NMR spectrum; (d) ¹H-¹³C-HSQC-NMR spectrum; (e) ¹H-¹³C-HMBC-NMR spectrum; (f) ¹H-¹H-ROESY-NMR spectrum.

regiochemical determination and stereochemical assignment are shown in Figs. 1–4.

2.2.1. Regiochemical assignment of **5b** as a model example

Examination of the ^{13}C -CRAPT (Fig. 1, spectrum b) and ^{13}C NMR spectra (Fig. S33) revealed the presence of 38 signals (16 aromatic CH's, 12 aromatic quaternary carbons, three carbonyl carbons, two spiro carbons, three methylene and two methine carbons, consistent with all carbon atoms being magnetically nonequivalent. The three carbonyl carbons of the pyrene and oxindole rings absorb at δ 202.0 (C_{10}), 177.2 (C_2 , identified via ^1H - ^{13}C -HMBCAD long-term coupling with $\text{N}_1\text{-H}$; Fig. 1, spectrum e), and 172.2 ($\text{C}_{2'}$, identified via ^1H - ^{13}C -HMBCAD long-term coupling with $\text{N}_{1'}\text{-H}$) ppm, respectively. The two spirocyclic carbon atoms of the pyrrolizidine ring C_3/C_3' (δ 77.1 ppm) and C_2/C_2' (δ 66.7 ppm) exhibit the broadest chemical shifts compared to the remaining carbon atoms of this particular ring. The chemical shifts and signals of these quaternary carbons were identified by comparing the ^{13}C NMR (Fig. S33) and ^{13}C -CRAPT spectra (Fig. 1, spectrum b). While the ^{13}C chemical shifts of the two methine carbons ($\text{C}_{1'}/\delta$ 56.7 & $\text{C}_{7a'}/\delta$ 65.4 ppm) were clearly identified as the only signals with negative phases in the aliphatic region of the ^1H - ^{13}C -HSQCAD spectrum (Fig. 1, spectrum d), the attached protons $\text{C}_{1'}\text{-H}$ and $\text{C}_{7a'}\text{-H}$ appear as d and ddd [δ 5.52 (d, $J = 8.0$ Hz, 1H, $\text{C}_{1'}\text{-H}$), 4.76 (ddd, 1H, $J = 10, 8.0, 5.6$ Hz, $\text{C}_{7a'}\text{-H}$) ppm, respectively] (Fig. 1, spectrum a) and were correlated in the ^1H - ^{13}C -HSQCAD NMR spectrum by two contours with the corresponding $\text{C}_{1'}$ and $\text{C}_{7a'}$ carbons at 56.7 ($\text{C}_{1'}\text{-H}$) and 65.4 ($\text{C}_{7a'}\text{-H}$) ppm, respectively (Fig. 1,

spectrum d). In particular, the $\text{C}_{1'}\text{-H}$ proton resonance of methine (δ 5.52), which is the lowest aliphatic signal in the ^1H NMR spectrum due to diamagnetic anisotropy, shows strong ^1H - ^{13}C HMBC correlations (Fig. 1, spectrum e) with the neighboring carbonyl group (C_{10} , δ 202 ppm, $^2J_{\text{CH}}$), the C_2/C_2' carbon of the spirocenter (66.7 ppm, $^2J_{\text{CH}}$), and the oxindole carbonyl $\text{C}_{2'}$ carbon (δ 172.2 ppm, $^3J_{\text{CH}}$), $\text{C}_7\text{-CH}_2$ (31.1 ppm, $^3J_{\text{CH}}$), and C_9' carbon (126.3 ppm, $^3J_{\text{CH}}$), (Fig. 1, spectrum e). The ^1H - ^{13}C -HMBC data of $\text{N}_{1'}\text{-H}$ of the oxindole ring was key in assigning the chemical shift values of all the carbon atoms associated with the 5-membered oxindole ring ($\text{C}_{2'}$, $\text{C}_{3'}$, $\text{C}_{8'}$ & $\text{C}_{9'}$), while the observed ^1H - ^1H -ROESYAD correlation contours between $\text{N}_{1'}\text{-H}$ and $\text{C}_{7'}\text{-H}$ (Fig. 1, spectrum f) assigned the chemical shift of the latter and prompted a partial assignment of the $\text{C}_{4'}\text{-C}_{7'}$ protons. Consequently, based on the ^1H - ^1H -gCOSYAD correlation of $\text{C}_{7'}\text{-H}$ (outside the diagonal contour at δ 6.09/7.19) (Fig. 1, spectrum c), the triplet at δ 7.19 was correlated with the neighboring proton $\text{C}_{6'}\text{-H}$. The most diagnostic resonance peaks for distinguishing the regioisomers were those associated with the methine groups ($\text{C}_{1'}\text{-H}$ & $\text{C}_{7a'}\text{-H}$) and their corresponding multiplicities. Based on the demonstrated vicinal correlations between $\text{C}_{1'}\text{-H}$ and $\text{C}_{7a'}\text{-H}$ in the ^1H - ^1H -gCOSYAD (Fig. 1, spectrum c), it is evident that the methine groups are spin-coupled. This obviously supports the suggested structure **5b** (Scheme 1) and rules out the regioisomer **6b**, in which the two groups are in separate spin systems. Literature evidence in line with our findings and supporting the regiochemical outcome of the above transformation stems from the work of Velikorodov *et al.* who described a similar

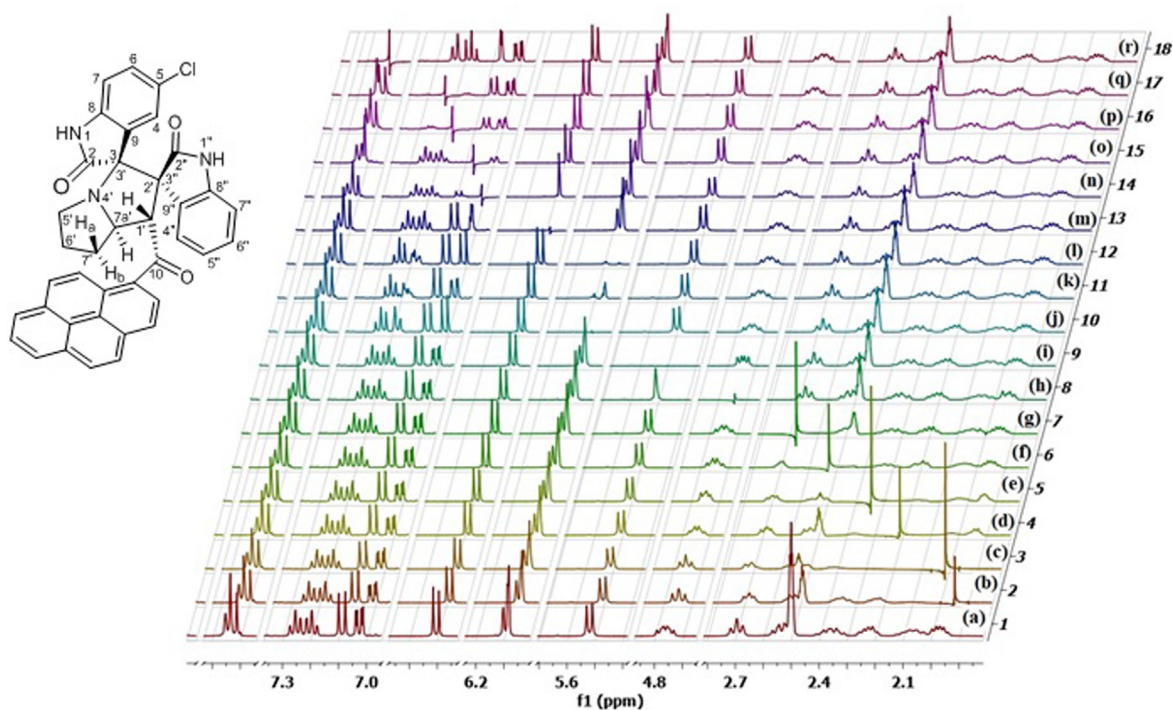


Fig. 2 ^1H - ^1H decoupling experiments of **5b**: (a) non-decoupled spectrum; (b) irradiation of $\text{C}_{7'}\text{-H}_b$; (c) irradiation of $\text{C}_6\text{-H}$; (d) irradiation of $\text{C}_6\text{-H}$; (e) irradiation of $\text{C}_7\text{-H}_a$; (f) irradiation of $\text{C}_5\text{-H}$; (g) irradiation of $\text{C}_5\text{-H}$; (h) irradiation of $\text{C}_{7a'}\text{-H}$; (i) irradiation of $\text{C}_{1'}\text{-H}$; (j) multiple-frequency irradiation of $\text{C}_4\text{-H}$ & $\text{C}_{7'}\text{-H}$; (k) irradiation of $\text{C}_{7'}\text{-H}$; (l) irradiation of $\text{C}_4\text{-H}$; (m) irradiation of $\text{C}_7\text{-H}$; (n) irradiation of $\text{C}_6\text{-H}$; (o) irradiation of $1\text{H}_{\text{pyrene}}$; (p) irradiation of $\text{C}_6'\text{-H}$; (q) irradiation of $\text{C}_5'\text{-H}$; (r) irradiation of $\text{C}_{4'}\text{-H}$ & $1\text{H}_{\text{pyrene}}$.

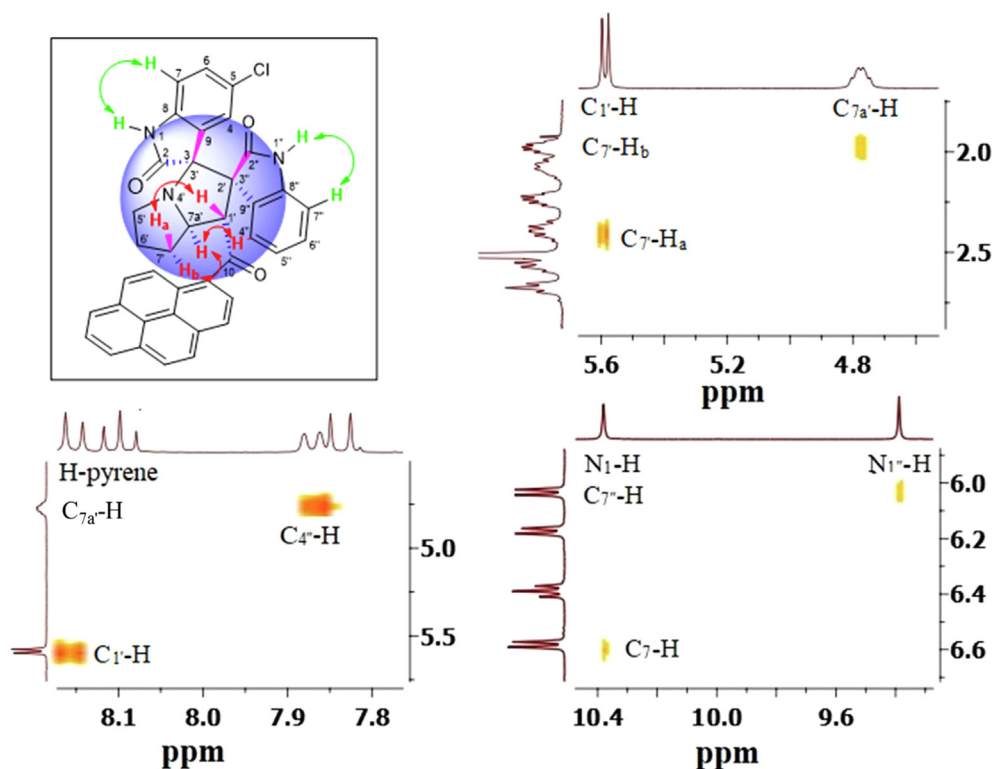


Fig. 3 (a) Overview of pertinent correlations observed in the ^1H - ^1H -ROESYAD spectrum of **5b** showing truncated signals stemming from $\text{C}_{1'}\text{-H}$, $\text{C}_{7\text{a}'}\text{-H}$, $\text{C}_{7'}\text{-H}_\text{a}$ and $\text{C}_{7'}\text{-H}_\text{b}$, $\text{N}_1\text{-H}$, $\text{N}_{1''}\text{-H}$, $\text{C}_7\text{-H}$, and $\text{C}_{7''}\text{-H}$.

cycloaddition to the one discussed herein using L-proline and isatin, although they utilized methyl 4-[2-(2-oxo-1,2-dihydro-3H-indol-3-ylidene)acetyl]phenylcarbamate as the dipolarophile (Velikorodov et al., 2011). Using unsubstituted isatin, the group reported the same regioisomeric outcome presented herein for the formation of the pyrrolizidine core, although the study was severely limited in substrate scope, reporting only one regioisomeric pyrrolizidine product without any stereochemical analysis. Later, the same group described an intriguing cycloaddition regioselectivity reversal associated with the same reaction when 5,7-dimethylisatin was used to generate the dipole instead of isatin (Velikorodov et al., 2013). The reversal observed was attributed to steric factors related to the hindered nature of 5,7-dimethylisatin. It is noted that the study reported only one regioisomeric product of this reversed type and the study was mostly focused on the preparation of other spiro cycloadducts like isoxazoline and pyrazole fragments. The stereochemical outcome was not discussed either. Another similar strategy to prepare the related octahydroindolizine through a 1,3-dipolar cycloaddition reaction of heteroaromatic *N*-ylides with 3-[(*E*)-2-aryl(heptyl)-2-oxoethylidene]indolin-2-ones also produced the same regiochemical outcome observed in our case (Serov et al., 2005). Although in their study the general structure of the dipolarophile offered similar electronic environment to the one utilized herein, both the dipolarophile and dipole are significantly different than those employed in our current study.

Although at the moment a more fundamental and tangible understanding of the reasons behind the selectivity observed could not be provided in a complete convincing manner, the current regiospecific cycloaddition reaction reported herein

of the dipole generated from isatin and L-proline to (*E*)-3-(2-oxo-2-(pyren-1-yl)ethylidene)indolin-2-ones demonstrated consistent attack of the electron-rich carbon atom of the dipole upon the α -carbon of the enone. It is conceivable that a combination of electronic (formation of a highly delocalized enolate anion following the addition of the dipole to the α -carbon of the enone) and steric factors (preferential attack of the dipole at the secondary α -carbon as opposed to the more hindered β tertiary carbon) work together to dictate the preferential formation of the observed regioisomeric product as the sole product.

2.2.2. Stereochemical assignment of **5b** as a model example

It was crucial to assign at least all chemical shifts of the aromatic protons of the oxindole and pyrrolizidine rings before attempting any kind of stereochemical assignment. Overlaps between the signals warranted extensive 2D, 3D, and homonuclear decoupling studies. As expected, the $\text{C}_{7\text{a}'}\text{-H}$ (δ 4.76 ppm) multiplicity was a doublet of a doublet of a doublet (ddd) due to coupling with $\text{C}_{1'}\text{-H}$ and the neighboring nonequivalent diastereotopic $\text{C}_{7'}\text{-H}_\text{a}$ and $\text{C}_{7'}\text{-H}_\text{b}$ protons. The $\text{C}_{1'}\text{-H}$ proton resonated significantly further downfield and appeared as a doublet at δ 5.52 ppm (d, J = 8.0 Hz) due to scalar coupling with the neighboring $\text{C}_{7\text{a}'}\text{-H}$. The six non-equivalent pyrrolizidine methylene protons $\text{C}_{7'}\text{-H}_2\text{-C}_5\text{-H}_2$ were correlated to each other and to the same spin system of $\text{C}_{7\text{a}'}\text{-H}$ and $\text{C}_{1'}\text{-H}$ by ^1H - ^1H -gDQFCOSY (Fig. 1, spectrum c), and the chemical shifts of carbon-13 were also verified by ^1H - ^{13}C -gHSQCAD correlations (Fig. 1, spectrum d). Clearly, the magnetic anisotropy and inherent diastereotopic nature of the methylenes affected the chemical shifts of their carbon atoms, and the

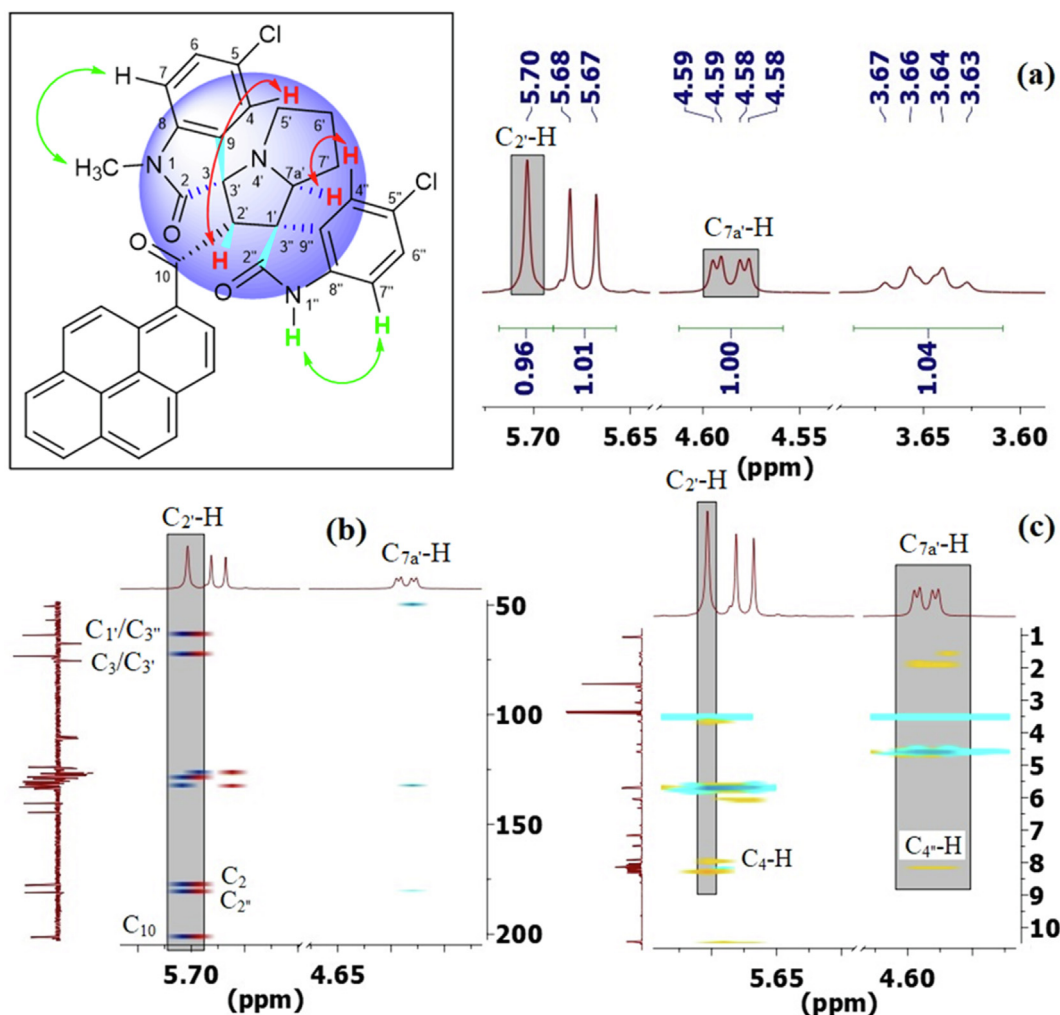


Fig. 4 (a) Relevant signals and correlations observed in the (a) ^1H , (b) ^1H - ^{13}C -HMBCAD, and (c) ^1H - ^1H -ROESYAD NMR spectra of **6i** showing truncated signals stemming from $\text{C}_2\text{-H}$ and $\text{C}_{7a'}\text{-H}$.

effect was even greater on the shift of their protons, offsetting the effect of the local atomic environment that justified the detailed NMR studies mentioned above. Fortunately, the $\text{N}_1\text{-H}$ group (δ 10.55 ppm) of the oxindole moiety (Figs. 1, ^1H NMR spectrum a) was the crucial access point that finally led to the unambiguous assignment of the relative stereochemistry of the four stereogenic centers of the isolated regioisomer. In the ROESYAD NMR spectrum (Fig. 1, spectrum f), there is a strongly correlated cross peak between the $\text{N}_1\text{-H}$ proton (δ 10.55 ppm) and $\text{C}_7\text{-H}$ (d, $J = 8.0$ Hz, δ 6.60 ppm) and the recognition of the latter triggered the partial assignment of $\text{C}_7\text{-H}$ and $\text{C}_6\text{-H}$ of the protons of the oxindole ring. The $\text{N}_1\text{-H}$ proton also showed strong ^1H - ^{13}C -HMBCAD correlation contours with C_7 ($^3J_{\text{CH}}$), C_2 ($^2J_{\text{CH}}$) and the C_3/C_3' spirocenter ($^3J_{\text{CH}}$), providing further evidence for the previous assignment and creating a perfect match between the previous signals and the corresponding oxindole ring atoms. It was expected that the presence of Cl would facilitate the assignment of the corresponding chemical shifts to the corresponding oxindole ring protons, as it produces a known distinct splitting pattern of the three aromatic protons as d

($\sim J = 8.0$ Hz), dd ($\sim J = 8.0, 2.4$ Hz) and d ($\sim J = 2.4$ Hz). Based on the ^1H - ^1H -gCOSY correlation of $\text{C}_7\text{-H}$ (contour at δ 6.60/7.02) (Fig. 1, spectrum c), the dd at δ 7.02 ($J = 8.0, 2.4$ Hz) was aligned with the neighboring $\text{C}_6\text{-H}$. Thus, it appears that the two overlapping signals between δ 6.12–6.07 ppm are from 2 protons belonging to two different aromatic oxindole rings, and that the overlapping signals in the δ 7.88–7.80 ppm belong to 2 protons from the oxindole and pyrenoyl rings (vide infra). From the ROESYAD NMR spectrum (Fig. 1, spectrum f), the strong correlation contour between the $\text{N}_1\text{-H}$ proton (δ 9.47 ppm) and δ 6.09 ppm $\text{C}_{7''}\text{-H}$ (d, $J = 8.0$ Hz) exposes it as one of the overlapping signals in the δ 6.12–6.07 region and prompts a partial assignment of the $\text{C}_{6''}\text{-H}$ and $\text{C}_{5''}\text{-H}$ protons. As can be seen from the contours at δ 7.19/6.09 and δ 7.19/7.25, the two triplet doubles at δ 7.19 and δ 7.25 ppm were assigned to $\text{C}_{6''}\text{-H}$ and $\text{C}_{5''}\text{-H}$, respectively.

Unfortunately, the most informative ^1H NMR signals of $\text{C}_{4''}\text{-H}$ and $\text{C}_4\text{-H}$, which incidentally have been previously used in related systems (Hussein and Abdel-Monem, 2011) as keys to assign the relative stereochemistry of all chiral cen-

ters, were part of the overlapping signals at δ 6.12–6.07 and δ 7.86–7.80 ppm, respectively, and eluded unambiguous identification because the 2D and 3D NMR data were insufficient to verify which signal belonged to which oxindole ring. Therefore, further advanced NMR studies were required, which could only be performed by ^1H - ^1H homonuclear uncoupling NMR experiments (vide infra).

Of note is the overlap between the two resonances at δ 7.80–7.84 ppm and two other signals at δ 6.08–6.09 ppm. ^1H - ^1H -gDQFCOSY correlations were insufficient to fully correlate the $\text{C}_4\text{-H}$ - $\text{C}_7\text{-H}$ spin system and distinguish between ^1H NMR signals associated with the latter and those originating from the other oxindole $\text{C}_{4'}\text{-H}$ - $\text{C}_{7'}\text{-H}$ spin system. Therefore, homonuclear uncoupling experiments (Fig. 2) were performed to assign the chemical shifts of the oxindole protons to their respective positions on the aromatic oxindole rings. Moreover, these experiments were of utmost importance in assigning the chemical shifts of the 6 aliphatic signals (δ 2.69–1.93 ppm) to their corresponding methylene protons. Thus, the irradiation of $\text{C}_7\text{-H}_b$ (Fig. 2, spectrum b), $\text{C}_6\text{-H}$ (Fig. 2, spectrum c), $\text{C}_{7'}\text{-H}$ (Fig. 2, spectrum d), $\text{C}_7\text{-H}_a$ (Fig. 2, spectrum e), $\text{C}_5\text{-H}$ (Fig. 2, spectrum f), $\text{C}_5\text{-H}$ (Fig. 2, spectrum g), $\text{C}_{7a'}\text{-H}$ (Fig. 2, spectrum h), $\text{C}_1\text{-H}$ (Fig. 2, spectrum i), $\text{C}_{7''}\text{-H}$ (Fig. 2, spectrum k), $\text{C}_4\text{-H}$ (Fig. 2, spectrum l), $\text{C}_7\text{-H}$ (Fig. 2, spectrum m), $\text{C}_6\text{-H}$ (Fig. 2, spectrum n), $\text{C}_{6'}\text{-H}$ (Fig. 2, spectrum p), $\text{C}_{5''}\text{-H}$ (Fig. 2, spectrum q), $\text{C}_{4''}\text{-H}$ & $1\text{H}_{\text{pyrene}}$ (Fig. 2, spectrum r), resulted in the collapse of prominent signals, including $\text{C}_5\text{-H}$, which collapsed to a doublet (spectrum c), $\text{C}_{7a'}\text{-H}$ to a doublet of doublets (spectrum i), and $\text{C}_1\text{-H}/\text{C}_4\text{-H}/\text{C}_7\text{-H}/\text{C}_{7''}\text{-H}/\text{C}_{4''}\text{-H}$ to singlet (spectrum h, n, p, & q, respectively). These experiments led to a clear assignment of chemical shifts for the oxindoles and pyrrolizidine protons as well as for the overlapping resonances between δ 6.12–6.07 and δ 7.86–7.80 ppm. In particular, irradiation of the characteristic $\text{C}_6\text{-H}$ dd (Fig. 2, spectrum n) collapsed both signals of $\text{C}_4\text{-H}$, $\text{C}_7\text{-H}$ into singlets and indicated that the overlapping resonances in the δ 6.12–6.07 region comprise a doublet with small scalar coupling value ($\text{C}_4\text{-H}$, $J = 2.0$ Hz) that overlaps with another doublet with much larger coupling constant ($\text{C}_{7''}\text{-H}$, $J = 8.0$ Hz). Similarly, irradiation of the characteristic $\text{C}_{5''}\text{-H}$ td (δ 7.25 ppm) and $1\text{H}_{\text{pyrene}}$ d (δ 7.09 ppm) suggests that the overlapping resonances in the δ 7.86–7.80 region comprise two doublets ($\text{C}_{5''}\text{-H}$ & $1\text{H}_{\text{pyrene}}$). Accordingly, the $\text{C}_{4''}\text{-H}$ - $\text{C}_{7''}\text{-H}$ protons were associated with δ 7.84, 7.25, 7.19 and 6.09 ppm, respectively, and the $\text{C}_4\text{-H}$, $\text{C}_7\text{-H}$ and $\text{C}_6\text{-H}$ protons were associated with δ 6.08, 6.60 and 7.02 ppm, respectively. As expected, the first proton spin system showed two triplets and two doublets, while the second one comprised two doublets and one doublet of doublets, further supporting the above assignments.

Having identified and assigned chemical shifts in the proton spectrum for each H atom in the three aforementioned autonomous spin systems (oxindole and pyrrolizidine ring systems), we needed to examine the ROESYAD spectrum (Fig. 1, spectrum F) closely for notable spatial correlations that could be used to determine the relative stereochemistry of the four stereogenic centers. A strong contour at δ 7.84/4.76 ppm indicates a proximity of $\text{C}_{4''}\text{-H}$ and $\text{C}_{7a'}\text{-H}$ to each other (Fig. 3), suggesting that a *syn*-stereochemical relationship exists between

the aromatic oxindole ring and $\text{C}_{7a'}\text{-H}$, determining the relative stereochemistry for the $\text{C}_2/\text{C}_{3''}$ -spirocenter and $\text{C}_{7a'}\text{-H}$. Based on the *trans* geometry of the dipole, $\text{C}_1\text{-H}$ is expected to be *trans* to both flanking groups, the adjacent aromatic oxindole ring and $\text{C}_{7a'}\text{-H}$. The *trans*-stereochemical relationship between $\text{C}_1\text{-H}$ and $\text{C}_{7a'}\text{-H}$ is evident from the lack of a cross-peak between their signals in the ROESYAD spectrum (Fig. 1, spectrum F). While $\text{C}_{7a'}\text{-H}$ showed a strong ROESY correlation with *cis* $\text{C}_7\text{-H}_b$ and no correlation with *trans* $\text{C}_7\text{-H}_a$, $\text{C}_1\text{-H}$ correlated strongly with $\text{C}_7\text{-H}_a$ and showed no correlation with $\text{C}_7\text{-H}_b$. The diastereotopic protons $\text{C}_7\text{-H}_a$ and $\text{C}_7\text{-H}_b$ were identified via ^1H - ^{13}C -HSQCAD NMR (Fig. 1, spectrum d), as they were both traced to a common carbon atom (δ 31.3 ppm), and their relative position with respect to $\text{C}_6\text{-H}_2$ and $\text{C}_5\text{-H}_2$ was determined via gDQFCOSY NMR (Fig. 1, spectrum c). Finally, the *trans* geometry of the oxindole rings was evident from the complete absence of relevant contours between the two groups of aromatic spin systems. Except for two cases (Table 1, entries 8 and 9), regioisomer **5** was obtained exclusively as pure (Table 1, entries 1, 2, 4, 5, 10, and 12) or as the major product (Table 1, entries 3, 6, 7, and 11), and regioisomer **6** was observed as a minor product. However, regioisomer **6** was obtained in pure form in one case (Table 1, entry 9) and as the major isomer (73%) in another example (Table 1, entry 8).

The regiochemistry of the cycloadduct **6i** was readily established due to the lack of correlation between $\text{C}_2\text{-H}$ (s) and $\text{C}_{7a'}\text{-H}$ (dd) in the ^1H - ^1H -gDQFCOSY and the pronounced multiplicity of $\text{C}_2\text{-H}$ (s) (Fig. 4, spectrum a), which, as expected, appears as the only singlet in the entire ^1H NMR spectrum (δ 5.70 ppm), being the only isolated aliphatic spin system in the entire molecule. Further evidence for the assignment of $\text{C}_2\text{-H}$ in cycloadduct **6i** is provided by a strong ^1H - ^{13}C -HMBCAD correlation of $\text{C}_2\text{-H}$ with the three flanking carbons at δ 72.1 ($\text{C}_3/\text{C}_{3'}$, $^2J_{\text{CH}}$), 62.7 ($\text{C}_1/\text{C}_{3''}$), and 200.3 (q, C_{10}), and with the two indoline carbonyls at 179.9 ($\text{C}_{2''}$, $^3J_{\text{CH}}$) and 176.6 (C_2 , $^3J_{\text{CH}}$) (Fig. 4, spectrum b). In the ^1H - ^1H -ROESYAD spectrum (Fig. 4, spectrum c), a strong correlation between the $\text{N}_{1''}\text{-H}$ and the $\text{C}_{7''}\text{-H}$ triggered the assignment of $\text{C}_{7''}\text{-H}$ - $\text{C}_{4''}\text{-H}$ using ^1H - ^1H -gDQFCOSY. Similarly, a strong correlation between $\text{N}_1\text{-CH}_3$ and $\text{C}_7\text{-H}$ in the ^1H - ^1H -ROESYAD triggered the assignment of $\text{C}_7\text{-H}$ - $\text{C}_4\text{-H}$ using ^1H - ^1H -gDQFCOSY. After the identification of the H NMR chemical shifts for each proton in the above four autonomous spin systems (oxindole and pyrrolizidine ring systems), it only remained to look for significant spatial proximity contours in the ^1H - ^1H -ROESYAD spectrum (Fig. 4, spectrum c) to clarify the relative stereochemistry of the four chiral centers. Certainly, a characteristic contour at δ 7.92/5.70 ppm indicated the spatial proximity of $\text{C}_4\text{-H}$ and $\text{C}_2\text{-H}$ to each other (Fig. 3), suggesting that a *syn*-stereochemical relationship exists between the oxindole aromatic ring of $\text{C}_7\text{-H}$ - $\text{C}_4\text{-H}$ and $\text{C}_2\text{-H}$ and determines the relative stereochemistry for the $\text{C}_3/\text{C}_{3''}$ -spirocenter and $\text{C}_2\text{-H}$. Based on the *trans*-stereochemical geometry of the dipole, the aromatic ring $\text{C}_{7''}\text{-H}$ - $\text{C}_{4''}\text{-H}$ is expected to be *trans* to $\text{C}_2\text{-H}$. The stereochemistry of $\text{C}_{7a'}\text{-H}$ was determined from a strong ^1H - ^1H -ROESYAD cross-peak (at δ 8.14/4.59 ppm) between $\text{C}_{4''}\text{-H}$ and $\text{C}_{7a'}\text{-H}$ as *syn* to the aromatic ring $\text{C}_{7''}\text{-H}$ - $\text{C}_{4''}\text{-H}$.

2.3. Reaction mechanism

As suggested in Scheme 2 below, the regio- and stereochemistry for the formation of dispiropyrrrolizidine oxindoles **5a-l** and **6a-l** are described in terms of electronic factor and the repulsion force. The formation of regioisomer **5** occurs via “pathway A”, in which the nucleophilic carbon atom of the azomethine ylide (AY) attacks the α -carbon of ethylene derivative **4** through an “*exo*” transition state (*exo*-TS5, Scheme 2). In this case, *exo*-TS5 is more stable because the corresponding “*endo*” transition state (*endo*-TS5) requires more free activation energy than *exo*-TS5 due to the electrostatic repulsion between the *cis*-carbonyl groups, which increases the free activation energy. On the other hand, the formation of the other regioisomer **6** occurs via “pathway B”, in which the nucleophilic carbon atom of the azomethine ylide (AY) attacks the β -carbon of the ethylene derivatives **4** also via an “*exo*” transition state (*exo*-TS6, Scheme 2).

Moreover, the regiochemistry of this type of 32CA reaction can be illustrated by the secondary orbital interaction (SOI) of the carbonyl group orbitals of dipolarophiles **4a-d** with those of ylides **3a-c**, as shown in Scheme 2.

2.4. Theoretical studies

Hypothetically, the reaction could proceed via pathway A (α -attack) or pathway B (β -attack) and in both cases the orientation of the reactants could be *endo* or *exo*. Therefore, a theoretical study was carried out to determine the energetics of reaction pathways A and B through the *exo* and *endo* transition states for the formation of compounds **5a** and **6a** starting from **3a** and **4a**. The calculated free energy profile of the *exo* and *endo* transition states (*exo*-TS and *endo*-TS) and the products of reaction pathway A are shown in Fig. 5A. Fig. 5B shows the same for reaction pathway B. The calculated activation energies (E_a) and free energy values (ΔG) are listed in Table 2.

The stereoselectivity of the reaction can be explained on the basis of the activation energies for the formation of **5a** and **6a** via *exo*- and *endo*-TS. The activation energy for the formation of *exo*-**5a** is lower than that of *endo*-**5a** (Fig. 5A). Similarly, the activation energy for the formation of *exo*-**6a** is lower than that of *endo*-**6a** (Fig. 5B). Therefore, all reactions are stereospecific and yield the *exo* adduct as a single product in all cases. To explain the regioselectivity, we compared the activation energies for *exo*-**5a** and *exo*-**6a**. From the activation energies (Fig. 5, Table 2), it is evident that the reaction is regiospecific and yields only cycloadduct-**5** as a single product. It should be noted that the *exo*-**6a** isomer was energetically more stable than *exo*-**5a**, but due to the higher activation energy barrier, it could not form. For reactions (**3a** + **4a**), (**3a** + **4b**), (**3a** + **4d**), (**3b** + **4a**), (**3b** + **4b**) and (**3c** + **4d**), the reaction proved to be regiospecific and gave only cycloadduct-**5** as the sole product. Thus, the computational results agree well with the experimental results. The optimized geometries of the *exo*-transition state (*exo*-TS) in pathways A and B are shown in Fig. 5C and 5D, respectively. Global electron density transfer (GEDT) calculations were performed on

the transition states. The GEDT value of 0.15e at **5a-exo**-TS is consistent with a polar nature of the reaction.

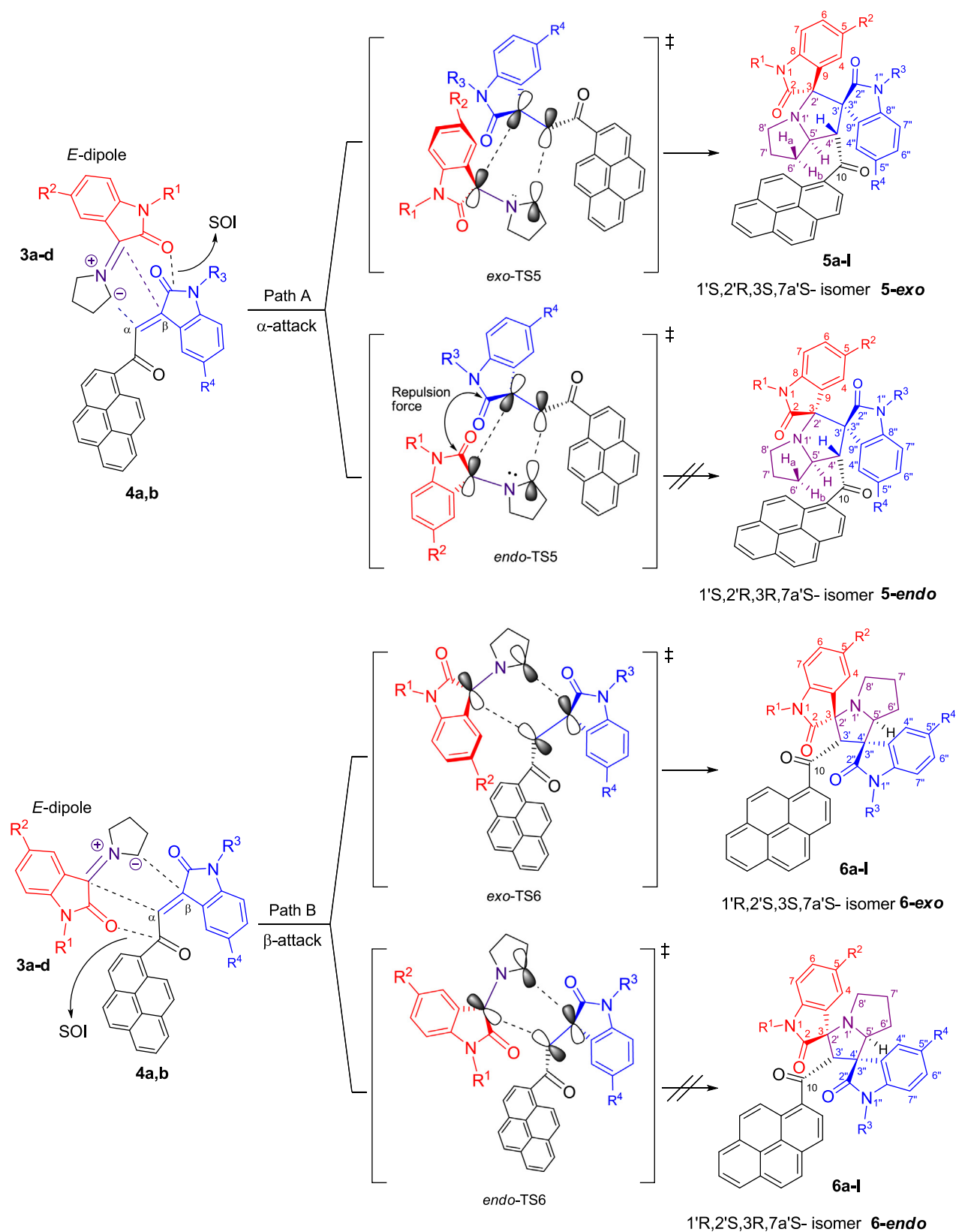
Experimentally, it was observed that in the case of reactions (**3a** + **4c**), (**3b** + **4d**), (**3c** + **4a**) and (**3c** + **4b**), the reaction was regioselective and cycloadduct-**5** was obtained as the major product and cycloadduct-**6** as the minor product in each case. To explain this observation, we calculated the free energy profile for reaction (**3a** + **4c**) as shown in Fig. 6. It is evident that the activation energy (Table 2) is lowest for the formation of cycloadduct-**5**, indicating that the formation of **5g** would be most favorable. The difference between the activation energies for the formation of *exo*-**5g** and *exo*-**6g** is 4.95 kcal/mol, which is less than the difference between the activation energies (5.32 kcal/mol) for the formation of *exo*-**5a** and *exo*-**6a**, which could be a reason for the formation of cycloadduct-**6** as a by-product.

In the case of (**3b** + **4c**) and (**3c** + **4c**), experiments have shown that the regiochemistry is reversed and the reaction is regioselective, yielding the cycloadduct-**6** (**6h**) as the major product in the case of (**3b** + **4c**), whereas in the case of (**3c** + **4c**) it is regiospecific, yielding only the cycloadduct-**6** (**6i**) as the single product. To explain this unique observation, the free energy profiles for both reactions were calculated (Figs. 7 and 8) and the activation energies are listed in Table 2.

However, the calculated activation energies for the formation of cycloadduct-**5** (**5h** and **5i**) are 4.99 and 4.60 kcal/mol, respectively, which are much lower than the activation energies for the formation of cycloadduct-**6** (10.05 and 9.45 kcal/mol for **6h** and **6i**, respectively). Thus, the calculated free energy profile could not explain the switching of regioselectivity in the case of (**3b** + **4c**) and (**3c** + **4c**). However, in all cases, the computational results confirmed that all reactions were stereospecific and, in all cases, gave the *exo*-adduct as a single product.

The optimized transition state geometries in the α -attack pathway show that the $C_4=C_5$ distance is smaller than the $C_2=C_3$ distance, indicating that the $C_4=C_5$ bond is formed first, followed by the formation of the $C_2=C_3$ bond. Similarly, the optimized transition state geometries in the β -attack pathway show that the $C_2=C_3$ distance is smaller than the $C_4=C_5$ distance, indicating that the formation of the $C_2=C_3$ bond is followed by the $C_4=C_5$ bond. To investigate whether there are stable intermediates, the $C_2=C_3$ distance in the α -attack pathway and the $C_4=C_5$ distance in the β -attack pathway were perturbed and the potential energy was plotted in Fig. 9. From the scan of the potential energy (PES), it can be seen that there is no stable intermediate in the β -attack and that after the formation of the $C_2=C_3$ bond, the $C_4=C_5$ bond is formed in a barrierless and concerted manner.

On the other hand, the α -attack pathway shows thermodynamically stable intermediates and a second transition state (Fig. 10). However, the activation energy required to form the intermediate is in the range of 0.1–0.3 kcal/mol, which is much less than the $k_B T$ at room temperature (0.59 kcal/mol), indicating that the intermediate is not stable at room temperature (as well as at the reaction temperature) and the α -attack also occurs in a concerted manner.



Scheme 2 Plausible mechanism for the formation of 1'-(1-pyrenoyl)-dispiro[indoline-3,3'-pyrrolizine-2',3''-indoline]-2,2''-diones **5a-l** and 2'-(1-pyrenoyl)-dispiro[indoline-3,3'-pyrrolizine-1',3''-indoline]-2,2''-diones **6a-l**.

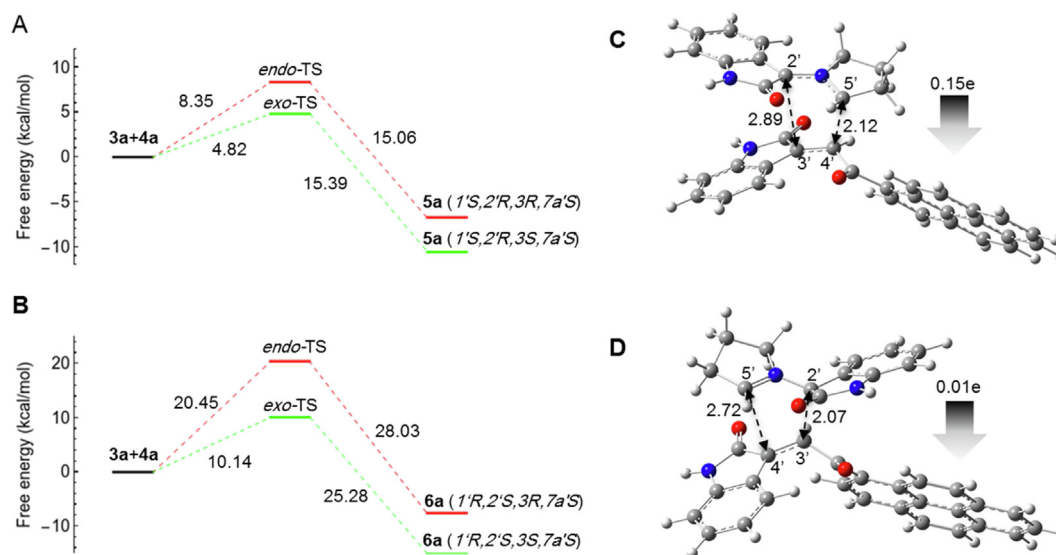


Fig. 5 Computed free energy profiles of the possible reaction paths for (**3a** + **4a**). (A) Free energies of α -attack (path A) for the formation of **5a** via *exo*- and *endo*-TS, respectively. Relative free energies are given in kcal/mol. (B) Free energies of β -attack (path B) for the formation of **6a** via *exo*- and *endo*-TS, respectively. Relative free energies are given in kcal/mol. Optimized geometries and global electron density transfer (GEDT) at *exo*-TS in α -attack (C) and β -attack (D). The 5'...4' and 2'...3' bond distances are shown with black dotted arrows. The gray arrow indicates the direction of GEDT.

Table 2 Computed activation energies and the free energies of selected reactions. Energy values are given in kcal/mol.

Reactants	Products	E_a	ΔG	Reactants	Products	E_a	ΔG
3a + 4a	<i>endo</i> - 5a	8.35	-6.71	3b + 4c	<i>endo</i> - 5h	8.72	-5.93
	<i>exo</i> - 5a	4.82	-10.57		<i>exo</i> - 5h	4.99	-9.30
	<i>endo</i> - 6a	20.45	-7.58		<i>endo</i> - 6h	20.45	-6.47
	<i>exo</i> - 6a	10.14	-15.14		<i>exo</i> - 6h	10.05	-14.58
3a + 4c	<i>endo</i> - 5g	7.10	-7.17	3c + 4c	<i>endo</i> - 5i	7.58	-6.48
	<i>exo</i> - 5g	3.85	-10.56		<i>exo</i> - 5i	4.60	-9.86
	<i>endo</i> - 6g	19.03	-8.03		<i>endo</i> - 6i	19.71	-6.93
	<i>exo</i> - 6g	8.80	-15.80		<i>exo</i> - 6i	9.45	-15.16

As described in our previous publication (Hussein et al., 2011), global and local reactivity descriptors such as chemical potential μ , chemical hardness η , and global electrophilicity ω , defined in the framework of density functional theory, have proven to be very useful for the interpretation of reactivity and regioselectivity in polar reactions. The calculated values of μ and η , ω are given in Table 3. From the data, it is evident that the electronic chemical potentials μ of **3a-c** are higher than those of **4a-d**. Moreover, the *E* configuration of **3a-c** has higher electronic chemical potential than its *Z* configuration and *E* configurations are energetically more favorable than the *Z* configurations. This suggests that electrons flow from the (*E*)-**3a-c** to the **4a-d**, which act as electrophiles due to their larger ω -values ($3.53 < \omega < 3.93$) compared to the ω -values ($1.52 < \omega < 1.87$) of the **3a-c**. On the electrophilicity scale (strong, $\omega > 1.5$ eV, moderate, $0.8 < \omega < 1.5$ eV, and marginal $\omega < 0.8$ eV) as described by Domingo et al. (Domingo et al., 2002), our ethylene derivatives **4a-d** can be counted among the strong molecules on this scale of electrophilicity.

However, **3a-c** are also strong electrophiles, but their electrophilicity is lower than that of **4a-d**. On the other hand, the nucleophilicity N index described by Jaramillo et al. (2008) classifies molecules as strong, $N > 3.00$ eV, moderate, 2.00 eV $< N < 3.00$ eV, and marginal nucleophilic, $N < 2.00$ eV. The calculated nucleophilicity descriptor N , as listed in Table 3, shows that all reactants can be classified as strong nucleophilic and (*E*)-**3a** is the best nucleophile in this series. These results confirm the expected reactivity pattern.

In order to rationalize and understand the regioselectivity observed in this work, we calculated the local reactivity indices, including the electrophilic and nucleophilic Parr and Fukui functions. The local electrophilicity parameter is defined by $\omega_k = \omega P_k^+$, to reveal the reactive behavior of the atoms forming a molecule. From Table 4, the highest values of P_k^- in **3a-c** at carbon atom C₇ are 0.388, 0.364 and 0.356, respectively. Moreover, the carbon C₁ in **4a** represents the electrophilic site with a local electrophilicity value of $\omega_k = 0.54$ eV. Therefore, the interaction takes place between

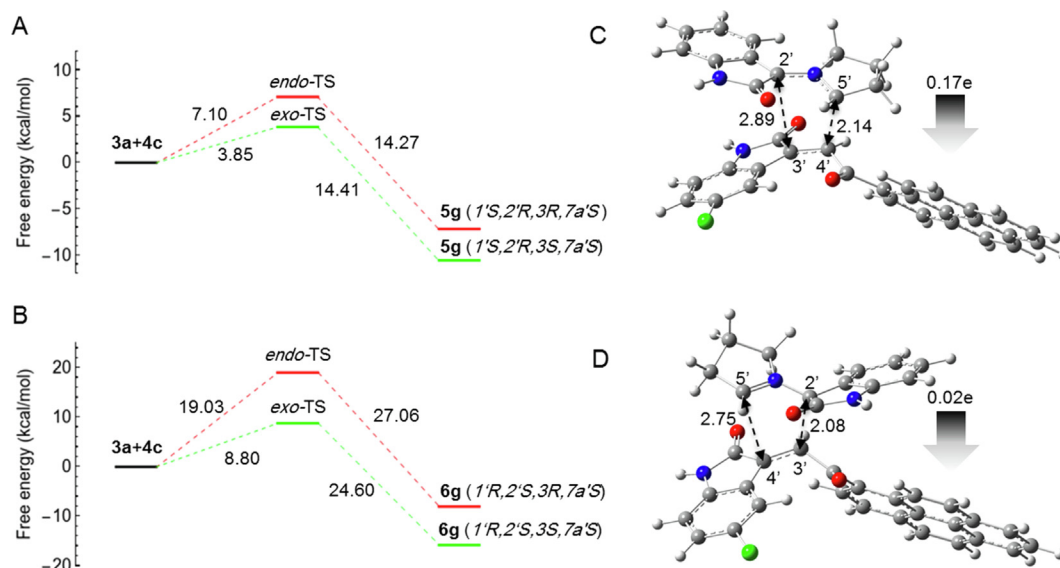


Fig. 6 Computed free energy profiles of the possible reaction paths for (**3a** + **4c**). (A) Free energies of α -attack (path A) for the formation of **5g** via *exo*- and *endo*-TS, respectively. Relative free energies are given in kcal/mol. (B) Free energies of β -attack (path B) for the formation of **6g** via *exo*- and *endo*-TS, respectively. Relative free energies are given in kcal/mol. (C) Optimized geometry of **5g**-*exo*-TS. (D) Optimized geometry of **6g**-*exo*-TS. The 5'...4' and 2'...3' bond distances are indicated with black dotted arrows. The gray arrow shows the direction of GEDT.

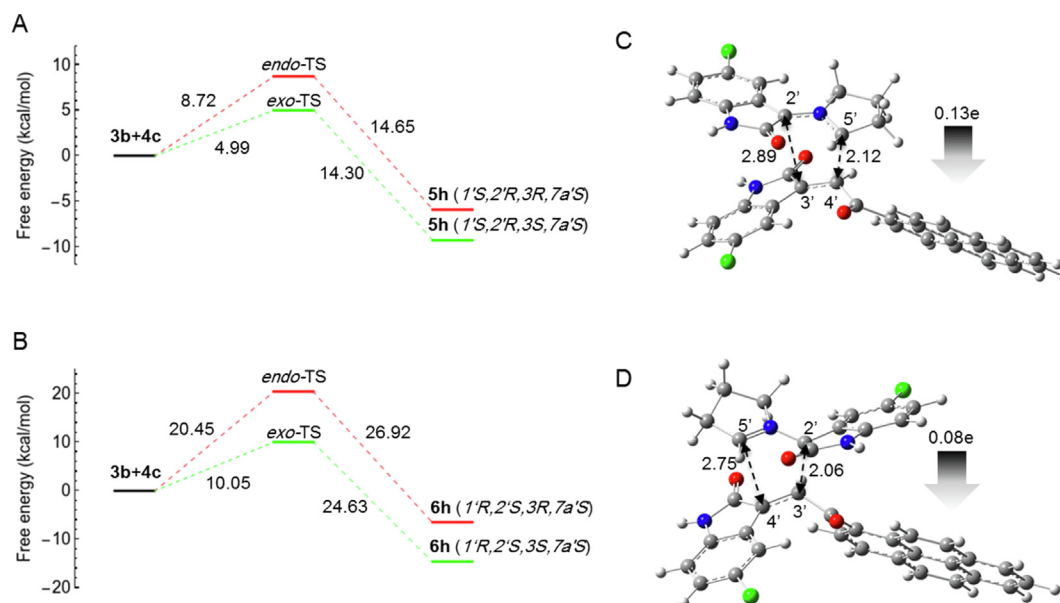


Fig. 7 Computed free energy profiles of the possible reaction paths for (**3b** + **4c**). (A) Free energies of α -attack (path A) for the formation of **5h** via *exo*- and *endo*-TS, respectively. Relative free energies are given in kcal/mol. (B) Free energies of β -attack (path B) for the formation of **6h** via *exo* and *endo* TS, respectively. Relative free energies are given in kcal/mol. (C) Optimized geometry of **5h**-*exo*-TS. (D) Optimized geometry of **6h**-*exo*-TS. The 5'...4' and 2'...3' bond distances are indicated with black dotted arrows. The gray arrow shows the direction of GEDT.

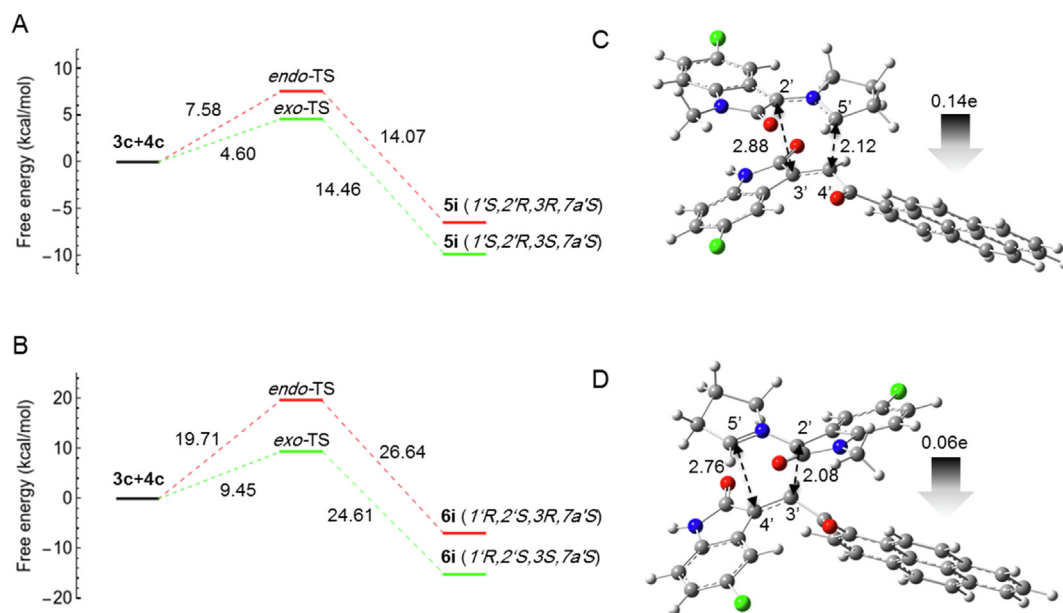


Fig. 8 Computed free energy profiles of the possible reaction paths for (**3c** + **4c**). (A) Free energies of α -attack (path A) for the formation of **5i** via *exo*- and *endo*-TS, respectively. Relative free energies are given in kcal/mol. (B) Free energies of β -attack (path B) for the formation of **6i** via *exo*- and *endo*-TS, respectively. Relative free energies are given in kcal/mol. (C) Optimized geometry of **5i**-*exo*-TS. (D) Optimized geometry of **6i**-*exo*-TS. The 5'...4' and 2'...3' bond distances are indicated with black dotted arrows. The gray arrow shows the direction of GEDT.

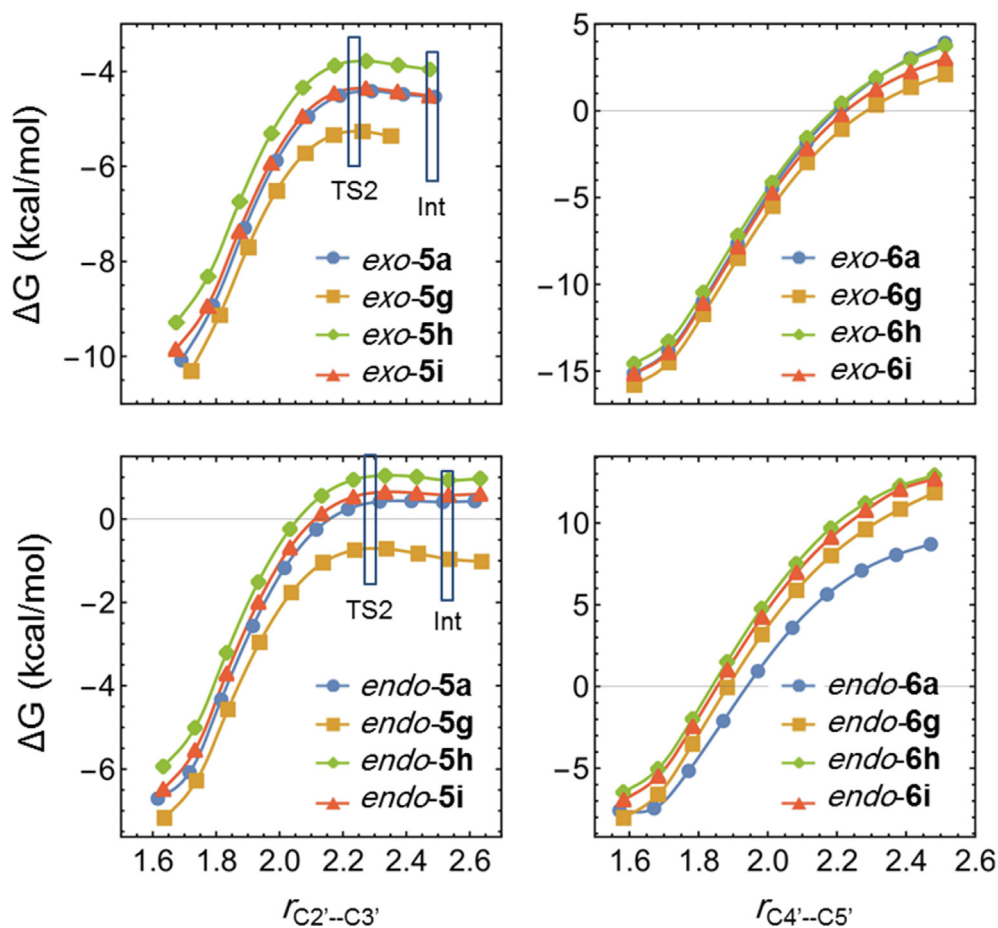


Fig. 9 Potential energy diagram for the $C_{2'}\cdots C_{3'}$ bond length perturbation in cycloadduct-5 and the $C_{4'}\cdots C_{5'}$ bond length perturbation in cycloadduct-6. Thermodynamically stable intermediate (Int) and the second transition state (TS2) are marked.

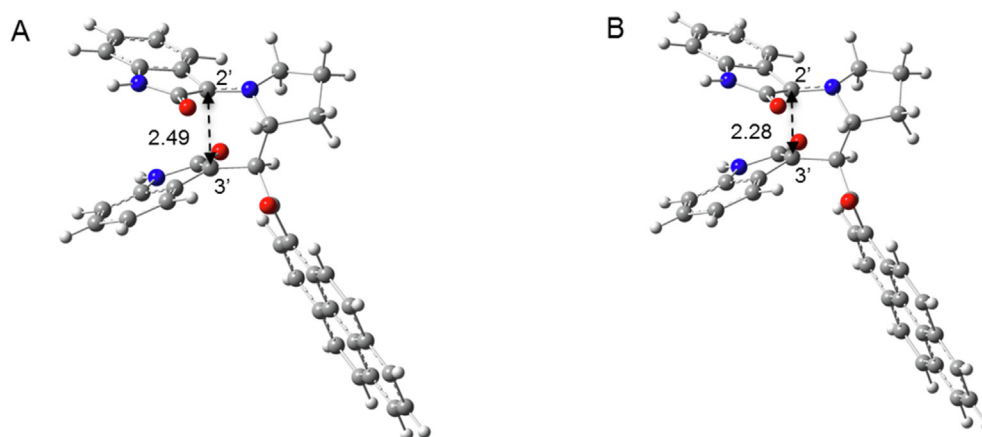


Fig. 10 Optimized geometry of the thermodynamically stable intermediate (A) and the second transition state (B) in the *exo-5a* formation path. $C_2=C_{3'}$ distances are shown with back dotted arrows.

Table 3 Global reactivity descriptors of the reactants.

Comp.	$E_{(\text{HOMO})}$	$E_{(\text{LUMO})}$	μ	η	ω	N
TCE	-9.41	-5.25	-7.33	4.16	6.47	0.00
4c	-5.89	-3.24	-4.57	2.65	3.93	3.52
4d	-5.87	-3.19	-4.53	2.68	3.82	3.54
4a	-5.82	-3.09	-4.45	2.74	3.62	3.59
4b	-5.80	-3.04	-4.42	2.76	3.53	3.61
(<i>Z</i>)- 3b	-5.15	-1.86	-3.51	3.29	1.87	4.26
(<i>Z</i>)- 3c	-5.10	-1.81	-3.46	3.29	1.81	4.31
(<i>E</i>)- 3b	-5.05	-1.72	-3.39	3.33	1.72	4.36
(<i>E</i>)- 3c	-5.00	-1.68	-3.34	3.32	1.68	4.41
(<i>Z</i>)- 3a	-4.93	-1.65	-3.29	3.28	1.65	4.48
(<i>E</i>)- 3a	-4.82	-1.52	-3.17	3.30	1.52	4.59

the C_7 center of **3a-c** and the C_1 center of **4a**, which facilitates the α -attack. Interestingly, in the case of **4c**, the C_2 carbon represents the electrophilic site with a local electrophilicity value of $\omega_k = 0.65$ eV, suggesting that the C_7 center of **3a-c** can align with the C_2 center of **4c**, facilitating β -attack. Although the activation energies could not clarify why cycloadduct-**6** was formed in some cases, the calculated descriptors for the local electrophilicity/nucleophilicity of the reactants could elucidate the mechanism of regioselectivity.

3. Conclusion

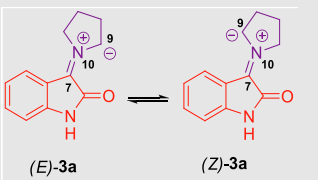
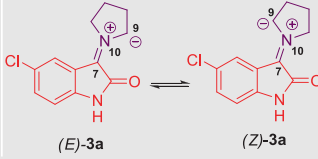
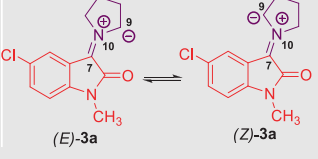
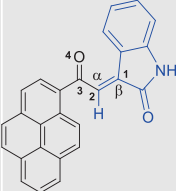
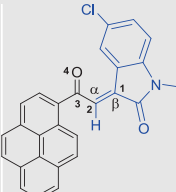
In conclusion, one-pot three-component regio- and stereoselective polar 32CA reactions of azomethine ylides with (*E*)-3-(2-oxo-2-(pyren-1-yl)ethylidene)indolin-2-one derivatives were carried out. The experimental results showed that the regiochemistry in these reactions is influenced by the chemical structure of both the dipole and the dipolarophile. A remarkable reversal of regioselectivity was carried out in the reaction of azomethine ylide generated by the reaction of L-proline and 5-chloroisatin or *N*-methyl-5-chloroisatin with (*E*)-5-chloro-3-(2-oxo-2-(pyren-1-yl)ethylidene)indolin-2-one. The chemical structures and stereochemistry of the obtained regioselective products were confirmed by 1D and 2D NMR spectroscopy.

Computational free energy profile studies clearly show that for both α -attack and β -attack, product formation via *exo*-TS always follows a lower energy pathway than the pathway via *endo*-TS, confirming the stereospecificity of the reactions and justifying the observation of the *exo*-adduct as a single product in all cases.

Generally, the reaction is regioselective affording adduct-**5** as major product via α -attack and the computational results agree well with the experimental observations. However, the calculated free energy profile could not explain the switching of regioselectivity in the case of dipole/dipolarophile interaction of 1-(5-chloro-2-oxoindolin-3-ylidene)pyrrolidinium ylide/(*E*)-5-chloro-3-(2-oxo-2-(pyren-1-yl)ethylidene)indolin-2-one and 1-(5-chloro-1-methyl-2-oxoindolin-3-ylidene)pyrrolidinium ylide/(*E*)-5-chloro-3-(2-oxo-2-(pyren-1-yl)ethylidene)indolin-2-one yielding the cycloadduct-**6** as the major product via β -attack.

Analysis of the optimized transition state geometries indicates that in the case of α -attack, the $C_4=C_5'$ bond is formed first, followed by the formation of the $C_2=C_3'$ bond, while in the case of β -attack, the $C_2=C_3'$ bond is formed first, followed by the formation of the $C_4=C_5'$ bond. PES analysis, as obtained by the $C_2=C_3'$ bond length perturbation in the case of α -attack, revealed the existence of an intermediate and a second transition state. However, the activation energy barrier for the second transition state is well below $k_B T$ at room temperature, indicating that the formation of the second bond in the α -

Table 4 Nucleophilic and electrophilic Fukui and Parr functions for the most relevant heavy atoms in the reactants.

	Comp.	Site k		f_k^-	f_k^+	P_k^-	P_k^+
 (E)-3a (Z)-3a	(Z)-3a	7	C	0.235	0.047	0.362	-0.102
		9	C	0.216	0.496	0.351	0.796
		10	N	0.007	0.166	-0.124	0.164
	(E)-3a	7	C	0.244	0.054	0.388	-0.095
		9	C	0.203	0.513	0.328	0.824
		10	N	0.006	0.160	-0.118	0.133
 (E)-3a (Z)-3a	(Z)-3b	7	C	0.229	0.034	0.349	-0.108
		9	C	0.199	0.503	0.315	0.803
		10	N	0.006	0.169	-0.116	0.162
	(E)-3b	7	C	0.241	0.040	0.364	-0.113
		9	C	0.191	0.517	0.300	0.826
		10	N	0.006	0.163	-0.111	0.133
 (E)-3a (Z)-3a	(Z)-3c	7	C	0.219	0.033	0.327	-0.109
		9	C	0.195	0.501	0.312	0.801
		10	N	0.006	0.170	-0.113	0.165
	(E)-3c	7	C	0.236	0.038	0.356	-0.124
		9	C	0.189	0.517	0.300	0.824
		10	N	0.006	0.163	-0.111	0.134
	4a	1	C	0.005	0.139	-0.004	0.149
		2	C	0.006	0.155	0.031	0.144
		3	C	0.003	0.136	-0.018	0.124
		4	O	0.022	0.126	-0.001	0.192
	4b	1	C	0.006	0.140	-0.007	0.150
		2	C	0.006	0.148	0.023	0.133
		3	C	0.001	0.139	-0.018	0.122
		4	O	0.020	0.127	-0.003	0.192
	4c	1	C	0.006	0.139	0.002	0.147
		2	C	0.005	0.168	0.015	0.166
		3	C	0.003	0.133	-0.018	0.117
		4	O	0.024	0.124	0.002	0.193
	4d	1	C	0.006	0.140	-0.003	0.137
		2	C	0.005	0.161	0.010	0.159
		3	C	0.003	0.137	-0.016	0.119
		4	O	0.023	0.125	-0.0001	0.193

attack is indeed barrierless at reaction temperature and the entire reaction proceeds in a concerted manner. PES analysis for the $C_4=C_5$ bond length disorder in the β -attack showed that the formation of the $C_4=C_5$ bond in the β -attack is barrierless and the reaction mechanism proceeds in a concerted manner, with a single transition state existing. Analysis of the global and local electrophilicity and nucleophilicity further elucidates the alignment of dipolarophiles **4a-d** with dipoles **3a-c** and highlights the regioselectivity of the reactions.

4. Experimental

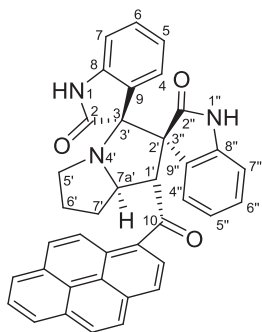
4.1. Chemical synthesis

All solvents used in this work were purchased from Sigma-Aldrich. They were all spectroscopic grade and used without additional purifications. Melting points of solids reported herein are uncorrected and were obtained using a Stuart SMP3 melting point apparatus. All NMR spectra were recorded on a Varian NMR machine (at 400 MHz for ^1H , 100 MHz for ^{13}C) in DMSO d_6 as solvent. The known dipolarophiles **4a-d** were synthesized according to literature procedure (Domingo, 2016).

4.1.1. Typical procedure for the preparation of 1'-(1-pyrenoyl)-dispiro[indoline-3,3'-pyrrolizidine-2',3''-indoline]-2,2''-diones **5a-l** and 2'-(1-pyrenoyl)-dispiro[indoline-3,3'-pyrrolizidine-1',3''-indoline]-2,2''-diones **6a-l**.

An ethanolic mixture (10 mL absolute ethanol) of isatin **1** (1.2 mmol), L-proline **2** (138 mg, 1.2 mmol) and **4** (1.0 mmol) was refluxed for 3–6 h, followed by cooling to room temperature. The resulting solid formed during the reaction was isolated by filtration to afford the corresponding regioisomers **5a-l** and **6a-l**. The molar ratio of **5a-l/6a-l** was determined by ^1H NMR spectroscopy. The pure cycloadducts **5a**, **5b**, **5d**, **5e**, **5j**, **5l**, and **6i** were obtained by recrystallization from absolute ethanol.

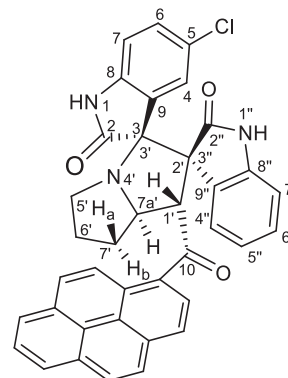
4.1.1.1. (1'S,2'R,3S,7a'S)-1'-(1-pyrenoyl)-dispiro[indoline-3,3'-pyrrolizidine-2',3''-indoline]-2,2''-diones (**5a**)



Buff crystals, mp 251–252 °C; yield 0.556 g (97%) from 176 mg (1.2 mmol) of **1a** and 373 mg (1.0 mmol) of **4a**. ^1H NMR (DMSO d_6 , 400 MHz) δ 10.40 (s, 1H, $\text{N}_1\text{-H}$), 9.41 (s, 1H, $\text{N}_{1''}\text{-H}$), 8.34 (d, $J = 8.0$ Hz, $1\text{H}_{\text{pyrene}}$), 8.30–8.25 (m, $3\text{H}_{\text{pyrene}}$), 8.22 (d, $J = 8.0$ Hz, $1\text{H}_{\text{pyrene}}$), 8.15 (d, $J = 8.0$ Hz, $1\text{H}_{\text{pyrene}}$), 8.10 (t, $J = 8.0$ Hz, $1\text{H}_{\text{pyrene}}$), 7.87

(d, $J = 7.2$ Hz, 1H, $\text{C}_{4''}\text{-H}$), 7.84 (d, $J = 9.2$ Hz, $1\text{H}_{\text{pyrene}}$), 7.24 (td, $J = 7.6, 0.8$ Hz, 1H, $\text{C}_{5''}\text{-H}$), 7.17 (td, $J = 7.6, 1.2$ Hz, 1H, $\text{C}_{6''}\text{-H}$), 7.09 (d, $J = 9.2$ Hz, $1\text{H}_{\text{pyrene}}$), 6.98 (td, $J = 7.6, 1.2$ Hz, 1H, $\text{C}_6\text{-H}$), 6.61 (d, $J = 7.6$ Hz, 1H, $\text{C}_7\text{-H}$), 6.42 (td, $J = 7.6, 1.2$ Hz, 1H, $\text{C}_5\text{-H}$), 6.20 (d, $J = 7.2$ Hz, 1H, $\text{C}_4\text{-H}$), 6.06 (d, $J = 7.1$ Hz, 1H, $\text{C}_{7''}\text{-H}$), 5.59 (d, $J = 8.0$ Hz, 1H, $\text{C}_{1''}\text{-H}$), 4.82–4.73 (m, 1H, $\text{C}_{7a''}\text{-H}$), 2.71–2.64 (m, 1H, $\text{C}_{5''}\text{-H}$), 2.60–2.54 (m, 1H, $\text{C}_{5''}\text{-H}$), 2.45–2.34 (m, 1H, $\text{C}_{7''}\text{-H}_a$), 2.28–2.20 (m, 1H, $\text{C}_{6''}\text{-H}$), 2.13–2.02 (m, 1H, $\text{C}_{6''}\text{-H}$), 2.01–1.94 (m, 1H, $\text{C}_{7''}\text{-H}_b$) ppm; ^{13}C NMR (DMSO d_6 , 100 MHz) δ 202.2 (q, C_{10}), 177.6 (q, C_2), 172.5 (q, $\text{C}_{2''}$), 142.5 (q, $\text{C}_{8''}$), 142.0 (q, C_8), 133.0 (q, C_{pyrene}), 132.7 (q, C_{pyrene}), 130.6 (q, C_{pyrene}), 129.9 (q, C_{pyrene}), 129.3 (C_6H), 129.2 ($\text{CH}_{\text{pyrene}}$), 129.1 ($\text{C}_{6''}\text{H}$), 128.0 ($\text{CH}_{\text{pyrene}}$), 127.7 (q, C_{pyrene}), 127.3 ($\text{CH}_{\text{pyrene}}$), 127.2 ($\text{CH}_{\text{pyrene}}$), 126.7 (q, $\text{C}_{9''}$), 126.6 ($\text{CH}_{\text{pyrene}}$), 126.1 ($\text{CH}_{\text{pyrene}}$), 125.8 ($\text{CH}_{\text{pyrene}}$), 125.7 (C_4H), 125.3 ($\text{CH}_{\text{pyrene}}$), 125.2 (q, C_9), 123.6 (q, C_{pyrene} and $\text{CH}_{\text{pyrene}}$), 123.5 ($\text{C}_{4''}\text{H}$), 123.4 (q, C_{pyrene}), 121.1 ($\text{C}_{5''}\text{H}$), 120.5 (C_5H), 109.4 ($\text{C}_{7''}\text{H}$), 109.1 (C_7H), 77.0 ($\text{C}_3/\text{C}_{3'}$), 66.7 ($\text{C}_2/\text{C}_{2''}$), 65.3 ($\text{C}_{7a''}\text{H}$), 56.9 ($\text{C}_{1''}\text{H}$), 46.9 ($\text{C}_5\text{-CH}_2$), 31.0 ($\text{C}_7\text{-CH}_2$), 30.2 ($\text{C}_6\text{-CH}_2$).

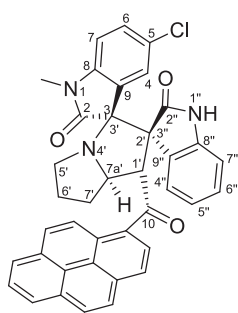
4.1.1.2. (1'S,2'R,3S,7a'S)-5-chloro-1'-(1-pyrenoyl)-dispiro[indoline-3,3'-pyrrolizidine-2',3''-indoline]-2,2''-diones (**5b**)



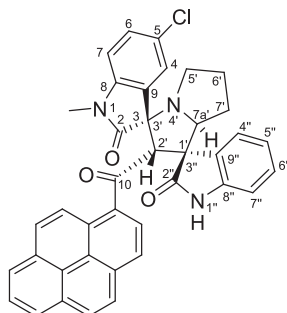
Pink crystals, mp 258–259 °C; yield 0.533 g (88%) from 218 mg (1.2 mmol) of **1b** and 373 mg (1.0 mmol) of **4a**. ^1H NMR (DMSO d_6 , 400 MHz) δ 10.55 (s, 1H, $\text{N}_1\text{-H}$), 9.47 (s, 1H, $\text{N}_{1''}\text{-H}$), 8.33 (d, $J = 8.0$ Hz, $1\text{H}_{\text{pyrene}}$), 8.29–8.24 (m, $3\text{H}_{\text{pyrene}}$), 8.20 (d, $J = 8.8$ Hz, $1\text{H}_{\text{pyrene}}$), 8.15 (d, $J = 8.0$ Hz, $1\text{H}_{\text{pyrene}}$), 8.08 (t, $J = 8.0$ Hz, $1\text{H}_{\text{pyrene}}$), 7.84 (d, $J = 6.8$ Hz, 1H, $\text{C}_{4''}\text{-H}$), 7.81 (d, $J = 9.6$ Hz, $1\text{H}_{\text{pyrene}}$), 7.25 (td, $J = 7.6, 0.8$ Hz, 1H, $\text{C}_{5''}\text{-H}$), 7.19 (td, $J = 7.6, 1.2$ Hz, 1H, $\text{C}_{6''}\text{-H}$), 7.09 (d, $J = 9.2$ Hz, $1\text{H}_{\text{pyrene}}$), 7.02 (dd, $J = 8.0, 2.4$ Hz, 1H, $\text{C}_6\text{-H}$), 6.60 (d, $J = 8.0$ Hz, 1H, $\text{C}_7\text{-H}$), 6.09 (d, $J = 8.0$ Hz, 1H, $\text{C}_{7''}\text{-H}$), 6.08 (d, $J = 2.0$ Hz, 1H, $\text{C}_4\text{-H}$), 5.52 (d, $J = 8.0$ Hz, 1H, $\text{C}_{1''}\text{-H}$), 4.76 (ddd, $J = 10, 8.0, 5.6$ Hz, 1H, $\text{C}_{7a''}\text{-H}$), 2.69 (t, $J = 8.0$ Hz, 1H, $\text{C}_{5''}\text{-H}$), 2.58–2.52 (m, 1H, $\text{C}_{5''}\text{-H}$), 2.42–2.30 (m, 1H, $\text{C}_{7''}\text{-H}_a$), 2.28–2.17 (m, 1H, $\text{C}_{6''}\text{-H}$), 2.14–2.01 (m, 1H, $\text{C}_{6''}\text{-H}$), 2.01–1.93 (m, 1H, $\text{C}_{7''}\text{-H}_b$) ppm; ^{13}C NMR (DMSO d_6 , 100 MHz) δ 202.0 (q, C_{10}), 177.2 (q, C_2), 172.2 (q, $\text{C}_{2''}$), 141.9 (q, $\text{C}_{8''}$), 141.4 (q, C_8), 132.8 (q, C_{pyrene}), 132.7 (q, C_{pyrene}), 130.6 (q, C_{pyrene}), 129.9 (q, C_{pyrene}), 129.4 ($\text{C}_{6''}\text{H}$), 129.2 (C_6H & $\text{CH}_{\text{pyrene}}$),

128.0 (C_{4''}H), 127.7 (C—Cl), 127.2 (2xCH_{pyrene}), 127.1 (q, C_{pyrene}), 126.7 (CH_{pyrene}), 126.3 (q, C_{9''}), 126.1 (CH_{pyrene}), 125.8 (2xCH_{pyrene}), 125.4 (C₄H), 124.6 (q, C₉), 123.6 (CH_{pyrene}), 123.5 (q, C_{pyrene}), 123.4 (q, C_{pyrene}), 123.3 (CH_{pyrene}), 121.2 (C_{5''}H), 110.5 (C₇H), 109.6 (C_{7''}H), 77.1 (C₃/C_{3'}), 66.7 (C₂/C_{3''}), 65.4 (C_{7a}H), 56.7 (C₁H), 46.9 (C₅—CH₂), 31.1 (C₇—CH₂), 30.2 (C₆—CH₂).

4.1.1.3. (1'S,2'R,3S,7a'S)-5-chloro-1-methyl-1'-(1-pyrenoyl)-dispiro[indoline-3,3'-pyrrolizidine-2',3''-indoline]-2,2''-diones (**5c**) and (1'R,2'S,3S,7a'S)-1-methyl-5-chloro-2'-(1-pyrenoyl)-dispiro[indoline-3,3'-pyrrolizidine-1',3''-indoline]-2,2''-diones (**6c**)



5c, 70%

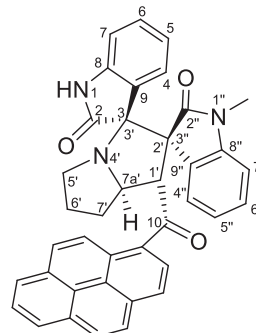


6c, 30%

Buff crystals, mp 177–178 °C; **5c**: yield 0.374 g (60%) from 235 mg (1.2 mmol) of **1c** and 373 mg (1.0 mmol) of **4a**. ¹H NMR (DMSO *d*₆, 400 MHz) δ 9.39 (s, 1H, N_{1''}—H), 8.41–8.02 (m, 7H_{pyrene}), 7.85 (d, *J* = 6.8 Hz, 1H, C_{4''}—H), 7.79 (d, *J* = 9.6 Hz, 1H_{pyrene}), 7.24 (td, *J* = 7.6, 0.8 Hz, 1H, C_{5''}—H), 7.17 (td, *J* = 7.6, 1.2 Hz, 1H, C_{6''}—H), 7.11 (dd, *J* = 8.0, 2.4 Hz, 1H, C₆—H), 7.05 (d, *J* = 9.2 Hz, 1H_{pyrene}), 6.81 (d, *J* = 8.0 Hz, 1H, C₇—H), 6.03 (d, *J* = 8.0 Hz, 1H, C_{7''}—H), 6.14 (d, *J* = 2.0 Hz, 1H, C₄—H), 5.52 (d, *J* = 8.0 Hz, 1H, C₁—H), 4.78 (ddd, *J* = 10, 8.0, 5.6 Hz, 1H, C_{7a}—H), 3.05 (s, 3H, N₁—CH₃), 2.65 (t, *J* = 8.0 Hz, 1H, C₅—H), 2.59–1.45 (m, 5H, C₅—H, C₆—H₂, C₇—H₂) ppm; ¹³C NMR (DMSO *d*₆, 100 MHz) δ 202.9 (q, C₁₀), 181.2 (q, C₂), 177.1 (q, C_{2''}), 143.9 (q), 140.7 (q), 133.6 (q), 133.0 (q), 132.1 (q), 130.8 (q), 130.6 (q), 130.2 (q), 130.1 (CH), 129.9 (q), 129.8 (CH), 128.6 (q), 127.9 (CH), 127.4 (CH), 127.3 (CH), 127.2 (CH), 127.1 (CH), 126.9 (CH), 126.8 (CH), 126.7 (CH), 126.6 (q), 125.8 (CH), 124.7 (CH), 124.5 (CH), 122.3 (CH), 110.3 (CH), 108.4 (C₇—H), 75.4 (CH), 72.5 (q), 67.0 (CH), 63.2 (q), 49.9 (CH₂), 26.6 (N₁—CH₃), 26.3 (CH₂), 24.5 (CH₂). **6c**: Yield (0.160 g, 26%) from 235 mg of **1c** and 373 mg of **4a**. ¹H NMR (DMSO *d*₆, 400 MHz) δ 10.32 (s, 1H, N_{1''}—H), 8.41–8.02 (m, 7H_{pyrene}), 7.87 (d, *J* = 2.0 Hz, 1H, C₄—H), 7.79 (d, *J* = 9.6 Hz, 1H_{pyrene}), 7.46 (dd, *J* = 8.0, 2.4 Hz, 1H, C₆—H), 7.14 (d, *J* = 8.0 Hz, 1H, C_{4''}—H), 7.05 (d, *J* = 9.2 Hz, 1H_{pyrene}), 6.42 (td, *J* = 7.6, 1.2 Hz, 1H, C_{5''}—H), 6.13 (td, *J* = 7.6, 1.2 Hz, 1H, C_{6''}—H), 5.76 (d, *J* = 8.0 Hz, 1H, C₇—H), 5.67 (s, 1H, C₂—H), 4.61 (dd, *J* = 8.4, 2.0 Hz, 1H, C_{7a}—H), 3.69–3.61 (m, 1H, C₅—H), 2.87 (s, 3H, N₁—CH₃), 2.59–1.45 (m, 5H, C₅—H, C₆—H₂,

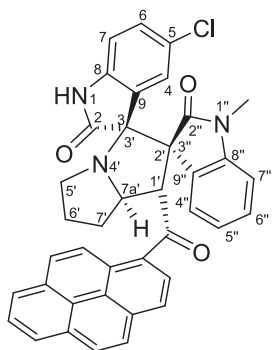
C₇—H₂) ppm; ¹³C NMR (DMSO *d*₆, 100 MHz) δ 200.7 (q, C₁₀), 176.0 (q, C₂), 172.6 (q, C_{2''}), 142.8 (q), 142.0 (q), 133.2 (q), 132.8 (q), 131.3 (q), 130.7 (q), 130.3 (q), 130.0 (q), 129.8 (CH), 129.6 (CH), 129.5 (CH), 128.7 (q), 128.4 (CH), 128.1 (q), 126.5 (CH), 126.4 (CH), 126.3 (q), 126.2 (CH), 125.9 (CH), 125.7 (CH), 125.2 (CH), 123.9 (CH), 123.7 (CH), 123.4 (CH), 123.2 (q), 121.7 (CH), 109.9 (CH), 109.7 (CH), 77.1 (q), 67.3 (q), 65.7 (CH), 57.1 (CH), 47.1 (CH₂), 31.2 (CH₂), 30.4 (CH₂), 26.2 (N₁—CH₃).

4.1.1.4. (1'S,2'R,3S,7a'S)-1''-methyl-1'-(1-pyrenoyl)-dispiro[indoline-3,3'-pyrrolizidine-2',3''-indoline]-2,2''-diones (**5d**)



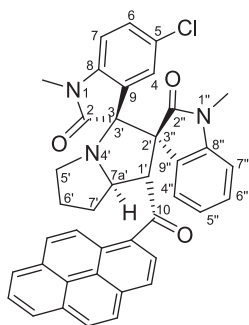
Yellow crystals, mp 183–184 °C; yield 0.475 g (81%) from 176 mg (1.2 mmol) of **1a** and 387 mg (1.0 mmol) of **4b**. ¹H NMR (DMSO *d*₆, 400 MHz) δ 10.39 (s, 1H, N₁—H), 8.32 (d, *J* = 7.2 Hz, 1H_{pyrene}), 8.29–8.23 (m, 3H_{pyrene}), 8.20 (d, *J* = 8.0 Hz, 1H_{pyrene}), 8.11 (d, *J* = 8.0 Hz, 1H_{pyrene}), 8.06 (t, *J* = 8.0 Hz, 1H_{pyrene}), 7.91 (d, *J* = 7.2 Hz, 1H, C_{4''}—H), 7.82 (d, *J* = 9.2 Hz, 1H_{pyrene}), 7.28 (td, *J* = 7.6, 0.8 Hz, 1H, C_{5''}—H), 7.16 (td, *J* = 7.6, 1.2 Hz, 1H, C_{6''}—H), 7.05 (d, *J* = 9.2 Hz, 1H_{pyrene}), 6.92 (td, *J* = 7.6, 1.2 Hz, 1H, C₆—H), 6.56 (d, *J* = 7.6 Hz, 1H, C₇—H), 6.38 (td, *J* = 8.0, 1.2 Hz, 1H, C₅—H), 6.24 (d, *J* = 7.2 Hz, 1H, C₄—H), 6.01 (d, *J* = 7.6 Hz, 1H, C_{7''}—H), 5.52 (d, *J* = 8.0 Hz, 1H, C₁—H), 4.79–4.72 (m, 1H, C_{7a}—H), 3.24 (s, 3H, N_{1''}—CH₃), 2.71–2.63 (m, 1H, C₅—H), 2.62–2.53 (m, 1H, C₅—H), 2.43–2.30 (m, 1H, C₇—H_a), 2.29–2.20 (m, 1H, C₆—H), 2.15–2.07 (m, 1H, C₆—H), 2.06–1.98 (m, 1H, C₇—H_b) ppm; ¹³C NMR (DMSO *d*₆, 100 MHz) δ 201.8 (q, C₁₀), 177.4 (q, C₂), 170.9 (q, C_{2''}), 142.7 (q, C_{8''}), 142.2 (q, C₈), 132.4 (q, C_{pyrene}), 132.1 (q, C_{pyrene}), 130.5 (q, C_{pyrene}), 129.2 (C₆—H), 129.1 (CH_{pyrene}), 129.0 (C_{6''}—H), 127.9 (CH_{pyrene}), 127.2 (q, C_{pyrene}), 127.1 (CH_{pyrene}), 127.0 (CH_{pyrene}), 126.9 (q, C_{pyrene}), 126.7 (CH_{pyrene}), 126.2 (CH_{pyrene}), 125.9 (CH_{pyrene}), 125.7 (C₄—H), 125.6 (q, C_{9''}), 125.1 (CH_{pyrene}), 124.8 (q, C₉), 124.0 (CH_{pyrene}), 123.9 (q, C_{pyrene}), 123.2 (C_{4''}—H), 123.0 (q, C_{pyrene}), 121.8 (C_{5''}—H), 120.4 (C₅—H), 109.1 (C_{7''}—H_b—H), 108.1 (C₇—H), 76.03 (C₃/C_{3'}), 65.9 (C₂/C_{3''}), 65.0 (C_{7a}—H), 57.3 (C₁—H), 46.6 (C₅—CH₂), 30.8 (C₇—CH₂), 30.0 (C₆—CH₂), 26.1 (N_{1''}—CH₃).

4.1.1.5. (1'S,2'R,3S,7a'S)-5-chloro-1''-methyl-1'-(1-pyrenoyl)-dispiro[indoline-3,3'-pyrrolizidine-2',3''-indoline]-2,2''-diones (**5e**)

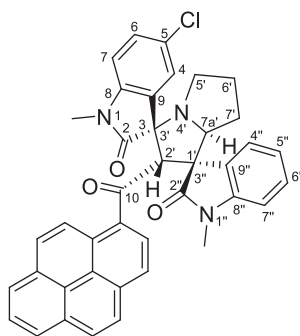


Yellow crystals, mp 239–240 °C; yield 0.466 g (75%) from 218 mg (1.2 mmol) of **1b** and 387 mg (1.0 mmol) of **4b**. ^1H NMR (DMSO d_6 , 400 MHz) δ 10.54 (s, 1H, $\text{N}_1\text{-H}$), 8.32–8.15 (m, 5H_{pyrene}), 8.11–8.01 (m, 2H_{pyrene}), 7.87 (d, $J = 7.2$ Hz, 1H, $\text{C}_{4''}\text{-H}$), 7.80 (d, $J = 9.2$ Hz, 1H_{pyrene}), 7.28 (td, $J = 7.6$, 0.4 Hz, 1H, $\text{C}_{5''}\text{-H}$), 7.16 (td, $J = 8.0$, 1.2 Hz, 1H, $\text{C}_{6''}\text{-H}$), 7.04 (d, $J = 9.2$ Hz, 1H_{pyrene}), 6.95 (dd, $J = 8.4$, 2.0 Hz, 1H, $\text{C}_6\text{-H}$), 6.55 (d, $J = 8.4$ Hz, 1H, $\text{C}_7\text{-H}$), 6.14 (d, $J = 2.0$ Hz, 1H, $\text{C}_4\text{-H}$), 6.03 (d, $J = 7.6$ Hz, 1H, $\text{C}_{7''}\text{-H}$), 5.44 (d, $J = 8.0$ Hz, 1H, $\text{C}_{1'}\text{-H}$), 4.73 (ddd, $J = 10$, 8.0, 5.6 Hz, 1H, $\text{C}_{7a'}\text{-H}$), 2.68 (t, $J = 8.4$ Hz, 1H, $\text{C}_5\text{-H}$), 2.56–2.50 (m, 1H, $\text{C}_5\text{-H}$), 2.38–2.26 (m, 1H, $\text{C}_7\text{-H}_a$), 2.28–2.17 (m, 1H, $\text{C}_{6'}\text{-H}$), 2.12–2.04 (m, 1H, $\text{C}_{6'}\text{-H}$), 2.04–1.98 (m, 1H, $\text{C}_7\text{-H}_b$), 1.60 (s, 3H, $\text{N}_{1''}\text{-CH}_3$) ppm; ^{13}C NMR (DMSO d_6 , 100 MHz) δ 201.4 (q, C_{10}), 176.8 (q, C_2), 170.4 (q, $\text{C}_{2''}$), 142.6 (q, $\text{C}_{8''}$), 141.0 (q, C_8), 132.3 (q, C_{pyrene}), 131.8 (q, C_{pyrene}), 130.2 (q, C_{pyrene}), 129.5 (q, C_{pyrene}), 129.3 (CH), 128.9 (CH), 127.8 (CH), 127.1 (q, C_{pyrene}), 126.8 (q, C_{pyrene}), 126.7 (CH), 126.5 (CH), 126.4 (CH), 126.4 (CH), 125.8 (CH), 125.6 (CH), 125.1 (q, C_{pyrene}), 125.1 (CH), 124.2 (C–Cl), 123.8 (q, C_{pyrene}), 123.1 (CH), 122.9 (q, C_{pyrene}), 122.8 (CH), 122.1 (CH), 121.7 (CH), 110.3 ($\text{C}_7\text{-H}$), 108.2 ($\text{C}_{7''}\text{-H}$), 76.3 (C_3/C_3'), 65.8 (C_2'/C_3''), 65.0 ($\text{C}_{7a'}\text{-H}$), 57.1 ($\text{C}_{1'}\text{-H}$), 46.5 ($\text{C}_5\text{-CH}_2$), 30.8 ($\text{C}_7\text{-CH}_2$), 29.9 ($\text{C}_{6'}\text{-CH}_2$), 26.0 ($\text{N}_{1''}\text{-CH}_3$).

4.1.1.6. (*1'S,2'R,3S,7a'S*)-5-chloro-1,1''-dimethyl-1'-(1-pyrenoyl)-dispiro[indoline-3,3'-pyrrolizidine-2',3''-indoline]-2,2''-diones (**5f**) and (*1'R,2'S,3S,7a'S*)-5-chloro-1,1''-dimethyl-2'-(1-pyrenoyl)-dispiro[indoline-3,3'-pyrrolizidine-1',3''-indoline]-2,2''-diones (**6f**)



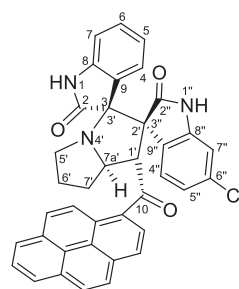
5f, 83%



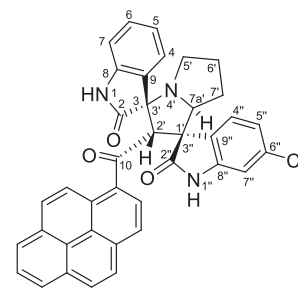
6f, 17%

Yellow crystals, mp 155–156 °C; yield 0.451 g (71%) from 235 mg (1.2 mmol) of **1c** and 387 mg (1.0 mmol) of **4b**. ^1H NMR (DMSO d_6 , 400 MHz) δ 8.61–5.97 (23.5H, Ar-H, both isomers), 5.66 (s, 0.47H, minor isomer), 5.49 (d, $J = 8.0$ Hz, 1H), 4.80 (ddd, $J = 10$, 8.0, 5.6 Hz, 1H), 4.66 (dd, $J = 8.4$, 2 Hz, 0.47H, minor isomer), 3.76–3.67 (m, 0.47H, minor isomer), 3.24 (s, 3H, CH_3 , major isomer), 3.08 (s, 1.42H, CH_3 , minor isomer), 2.75–1.60 (m, 8.33H, both isomers), 2.84 (s, 1.42H, CH_3 , minor isomer), 1.53 (s, 3H, CH_3 , major isomer) ppm; ^{13}C NMR (DMSO d_6 , 100 MHz) major isomer: δ 201.5 (q, C_{10}), 175.5 (q, C_2), 170.5 (q, $\text{C}_{2''}$), 142.8 (q), 142.6 (q), 132.7 (q), 132.0 (q), 130.5 (q), 129.8 (q), 128.2 (CH), 128.1 (CH), 127.4 (q), 127.0 (CH), 126.9 (CH), 126.8 (CH), 126.2 (CH), 126.0 (CH), 125.9 (CH), 125.3 (q), 125.1 (q), 125.1 (CH), 124.9 (CH), 124.1 (q), 123.4 (CH), 123.2 (q), 123.0 (CH), 122.9 (q), 122.6 (CH), 122.1 (CH), 109.6 (CH), 108.6 (CH), 76.3 (q), 72.2 (q), 65.3 (CH), 57.3 (CH), 49.8 (CH_2), 31.0 (CH_2), 30.3 (CH_2), 26.1 ($\text{N}_1\text{-CH}_3$), 24.9 ($\text{N}_1'\text{-CH}_3$).

4.1.1.7. (*1'S,2'R,3S,7a'S*)-5''-chloro-1'-(1-pyrenoyl)-dispiro[indoline-3,3'-pyrrolizidine-2',3''-indoline]-2,2''-diones (**5g**) and (*1'R,2'S,3S,7a'S*)-5''-chloro-2'-(1-pyrenoyl)-dispiro[indoline-3,3'-pyrrolizidine-1',3''-indoline]-2,2''-diones (**6g**).



5g, 59%

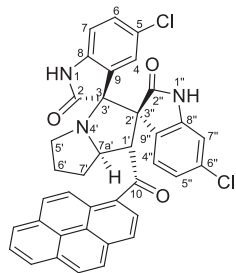


6g, 41%

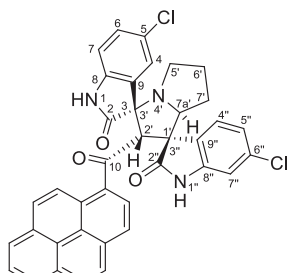
Pink crystals, mp 243–244 °C; yield 0.577 g (95%) from 176 mg (1.2 mmol) of **1a** and 408 mg (1.0 mmol) of **4c**. ^1H NMR (DMSO d_6 , 400 MHz) δ 10.64 (s, 0.69H, $\text{N}_{1''}\text{-H}$, minor), 10.44 (s, 1H, $\text{N}_{1''}\text{-H}$, major), 10.40 (s, 0.69H, $\text{N}_{1'}\text{-H}$, minor), 9.62 (s, 1H, $\text{N}_{1'}\text{-H}$, major), 8.66–6.98 (m, 22H, Ar-H), 6.62 (d, $J = 7.6$ Hz, 1H, major), 6.50 (t, $J = 7.6$ Hz, 1H, $\text{C}_6\text{-H}$, major), 6.22 (d, $J = 7.2$ Hz, 0.69H, $\text{C}_7\text{-H}$, minor), 6.12 (dd, $J = 8.0$, 2.0 Hz, 0.69H, $\text{C}_{5''}\text{-H}$, minor), 6.11 (d, $J = 8.4$ Hz, 1H, $\text{C}_{4''}\text{-H}$, major), 5.71 (d, $J = 8.4$ Hz, 0.69H, $\text{C}_{4''}\text{-H}$, minor), 5.57 (s, 0.69H, $\text{C}_{2''}\text{-H}$, minor), 5.58 (d, $J = 8.0$ Hz, 1H, $\text{C}_{1'}\text{-H}$, major), 4.66 (ddd, $J = 10$, 8.0, 5.6 Hz, 1H, $\text{C}_{7a'}\text{-H}$, major), 4.60 (dd, $J = 8.4$, 2 Hz, 0.69H, $\text{C}_{7a'}\text{-H}$, minor), 3.69–3.64 (m, 0.69H, minor), 2.69 (t, $J = 8.4$ Hz, 1H, $\text{C}_5\text{-H}$, major), 2.60 (t, $J = 8.4$ Hz, 0.69H, $\text{C}_5\text{-H}$, minor), 2.45–1.52 (m, 7.5H, both isomers) ppm; ^{13}C NMR (DMSO d_6 , 100 MHz) δ 202.2 (q, C_{10} , major), 200.4 (q, C_{10} , minor), 180.4 (q, $\text{C}_{2''}$), 178.9 (q, $\text{C}_{2''}$), 177.2 (q, C_2), 172.2 (q, C_2), 143.5 (q), 142.5 (q), 140.9 (q), 139.6 (q), 132.9, 132.7, 132.5, 132.2, 131.4, 129.9, 129.8, 129.7, 129.5 (2xC), 129.4, 129.3, 129.2, 128.9, 128.8, 128.2, 128.0 (2xC), 127.7, 127.6, 127.4, 127.2, 126.9 (2xC), 126.7, 126.6, 126.3,

126.2, 126.0, 125.9 (2xC), 126.2, 126.1, 126.0, 125.9 (2xC), 125.8, 125.6, 125.3, 125.1, 124.9, 124.7, 123.7, 123.6, 123.5, 123.4 (2xC), 123.0 (2xC), 121.2, 120.6, 110.7 (CH), 109.7 (CH), 109.3 (CH), 109.2 (CH), 76.8 (q, major), 74.7 (CH, minor), 72.6 (q, minor), 66.8 (q, major), 66.7 (CH, minor), 65.3 (CH, major), 63.1 (q, minor), 56.9 (CH, major), 49.6 (CH₂, minor), 46.38 (CH₂, major), 31.0 (CH₂, major), 30.0 (CH₂, major), 26.2 (CH₂, minor), 24.2 (CH₂, minor).

4.1.1.8. (1'S,2'R,3S,7a'S)-5,5''-dichloro-1'-(1-pyrenoyl)-dispiro[indoline-3,3'-pyrrolizidine-2',3''-indoline]-2,2''-diones (**5h**) and (1'R,2'S,3S,7a'S)-5,5''-dichloro-2'-(1-pyrenoyl)-dispiro[indoline-3,3'-pyrrolizidine-1',3''-indoline]-2,2''-diones (**6h**)



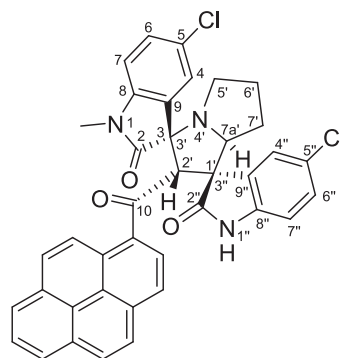
5h, 27%



6h, 73%

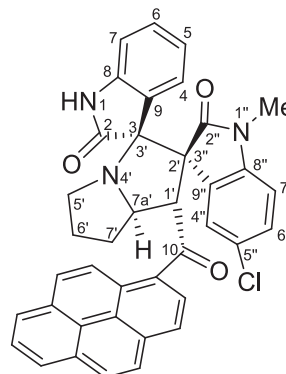
Buff crystals, mp 241–242 °C; **5h**: yield (0.158 g, 25%) from 218 mg (1.2 mmol) of **1b** and 408 mg (1.0 mmol) of **4c**. ¹H NMR (DMSO *d*₆, 400 MHz) δ 10.61 (s, 1H, NH), 9.70 (s, 1H, NH), 8.40–6.00 (m, 15H, Ar-H), 5.68 (d, *J* = 8.0 Hz, 0.1H, C_{1'}-H), 4.68 (ddd, *J* = 10, 8.0, 5.6 Hz, 1H, C_{7a'}-H), 2.72 (t, *J* = 8.4 Hz, 1H, C_{5'}-H), 2.42–1.50 (m, 5H, C_{5'}-H, C_{6'}-H₂, C_{7'}-H₂) ppm; ¹³C NMR (DMSO *d*₆, 100 MHz) δ 202.5 (q, C₁₀), 177.3 (q), 172.5 (q), 141.9 (q), 140.4 (q), 133.2 (q), 132.9 (q), 131.0 (q), 130.9 (q), 129.8 (CH), 129.7 (q, CH), 129.6 (CH), 129.0 (q), 128.1 (CH), 128.0 (q), 127.1 (CH), 127.1 (CH), 126.7 (CH), 126.6 (q, CH), 126.4 (q, CH), 126.3 (CH), 125.9 (q), 125.6 (q, CH), 124.1 (CH), 124.0 (q), 123.8 (CH), 123.4 (CH), 111.4 (CH), 111.2 (CH), 77.3 (q), 67.3 (q), 65.9 (CH), 57.3 (CH), 47.3 (CH₂), 31.5 (CH₂), 30.5 (CH₂). **6h**: Yield (0.426 g, 66%) from 218 mg of **1b** and 408 mg of **4c**. ¹H NMR (DMSO *d*₆, 400 MHz) δ 10.80 (s, 1H, NH), 10.43 (s, 1H, NH), 8.40–6.00 (m, 15H, Ar-H), 5.66 (s, 1H, C_{2'}-H), 4.57 (dd, *J* = 8.4, 2 Hz, 1H, C_{7a'}-H), 3.67–3.59 (m, 1H, C_{5'}-H), 2.61 (t, *J* = 8.4 Hz, 1H, C_{5'}-H), 2.42–1.50 (m, 4H, C_{6'}-H₂, C_{7'}-H₂) ppm; ¹³C NMR (DMSO *d*₆, 100 MHz) δ 201.1 (C₁₀, q), 180.7 (q), 179.1 (q), 142.8 (q), 140.1 (q), 133.3 (q), 132.7 (q), 131.8 (q), 130.2 (q), 130.0 (CH), 129.8 (CH), 129.7 (q, CH), 128.7 (CH), 128.5 (CH), 127.4 (CH), 127.3 (CH), 128.1 (q), 126.7 (CH), 126.6 (q, CH), 126.4 (q, CH), 126.2 (CH), 126.0 (CH), 125.6 (q, CH), 124.2 (CH), 123.8 (q), 123.7 (CH), 123.5 (q), 111.4 (CH), 109.6 (CH), 75.0 (CH), 73.2 (q), 67.2 (CH), 65.9 63.4 (q), 50.1 (CH₂), 26.6 (CH₂), 24.7 (CH₂).

4.1.1.9. (1'R,2'S,3S,7a'S)-5,5''-dichloro-1-methyl-2'-(1-pyrenoyl)-dispiro[indoline-3,3'-pyrrolizidine-1',3''-indoline]-2,2''-diones (**6i**)



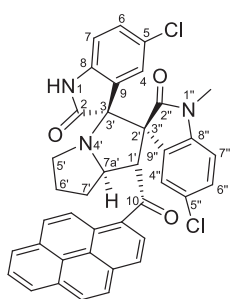
Yellow crystals, mp 230–231 °C; yield 0.512 g (78%) from 235 mg (1.2 mmol) of **1c** and 408 mg (1.0 mmol) of **4c**. ¹H NMR (DMSO *d*₆, 400 MHz) δ 10.43 (s, 1H, N_{1'}-H), 8.30 (d, *J* = 8.0 Hz, 2H_{pyrene}), 8.26 (d, *J* = 8.0 Hz, 1H_{pyrene}), 8.20 (d, *J* = 6.0 Hz, 1H_{pyrene}), 8.16 (d, *J* = 6.4 Hz, 1H_{pyrene}), 8.14 (d, *J* = 1.6 Hz, 1H, C_{4''}-H), 8.12–8.11 (m, 2H_{pyrene}), 8.07 (t, *J* = 4.8 Hz, 1H_{pyrene}), 8.04 (d, *J* = 6.0 Hz, 1H_{pyrene}), 7.92 (d, *J* = 1.2 Hz, 1H, C₄-H), 7.48 (dd, *J* = 5.6, 1.2 Hz, 1H, C₆-H), 7.17 (d, *J* = 5.6 Hz, 1H, C₇-H), 6.05 (dd, *J* = 5.6, 1.6 Hz, 1H, C_{6''}-H), 5.70 (s, 1H, C₂-H), 5.68 (d, *J* = 5.6 Hz, 1H, C_{7''}-H), 4.59 (dd, *J* = 6.0, 1.6 Hz, 1H, C_{7a'}-H), 3.65 (dd, *J* = 8.0, 4.0 Hz, 1H, C_{5'}-H), 3.39 (s, 3H, N₁-CH₃), 2.59 (t, *J* = 8.0 Hz, 1H, C₅-H), 1.95–1.88 (m, 1H, C₇-H), 1.87–1.80 (m, 1H, C₆-H), 1.69–1.60 (m, 1H, C₆-H), 1.59–1.50 (m, 1H, C₇-H) ppm; ¹³C NMR (DMSO *d*₆, 100 MHz) δ 200.3 (q, C₁₀), 179.9 (q, C_{2''}), 176.6 (q, C₂), 143.4 (q, C₈), 139.3 (q, C_{8''}), 132.6 (q, C_{9''}), 131.8 (q, C_{pyrene}), 130.9 (C–Cl), 130.1 (C–Cl), 129.5 (q, C_{pyrene}), 129.4 (C₆H), 129.1 (CH_{pyrene}), 128.1 (q, C_{pyrene}), 127.8 (CH_{pyrene}), 127.3 (q, C_{pyrene}), 126.7 (CH_{pyrene}), 126.6 (CH_{pyrene}), 126.4 (C_{6''}H), 126.0 (CH_{pyrene}), 125.9 (CH_{pyrene}), 125.8 (q, C_{9''}), 125.7 (C₄H), 125.6 (q, C_{pyrene}), 125.5 (CH_{pyrene}), 125.4 (C_{4''}H), 123.5 (CH_{pyrene}), 123.0 (q, C_{pyrene}), 122.9 (CH_{pyrene}), 122.73 (q, C_{pyrene}), 109.7 (C₇H), 108.9 (C_{7''}H), 74.4 (C_{7a'}H), 72.1 (C₃/C_{3''}), 66.5 (C₂H), 62.7 (C₁/C_{3''}), 49.4 (C₅-CH₂), 26.1 (N₁-CH₃), 25.9 (C₆-CH₂), 24.0 (C₆-CH₂).

4.1.1.10. (1'S,2'R,3S,7a'S)-5''-chloro-1''-methyl-1'-(1-pyrenoyl)-dispiro[indoline-3,3'-pyrrolizidine-2',3''-indoline]-2,2''-diones (**5j**)

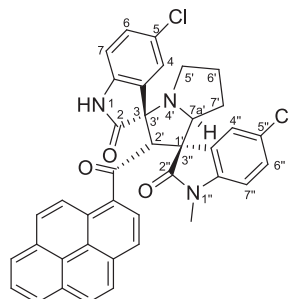


Pale yellow crystals, mp 262–263 °C; yield 0.516 g (83%) from 176 mg (1.2 mmol) of **1a** and 422 mg (1.0 mmol) of **4d**. ^1H NMR (DMSO d_6 , 400 MHz) δ 10.45 (s, 1H, $\text{N}_1\text{-H}$), 8.37–8.01 (m, 7 H_{pyrene}), 7.92 (d, $J = 9.6$ Hz, 1 H_{pyrene}), 7.84 (d, $J = 2.4$ Hz, 1H, $\text{C}_4''\text{-H}$), 7.22 (d, $J = 9.6$ Hz, 1 H_{pyrene}), 7.19 (dd, $J = 8.4, 2.4$ Hz, 1H, $\text{C}_6''\text{-H}$), 6.95 (td, $J = 7.6, 0.8$ Hz, 1H, $\text{C}_6\text{-H}$), 6.59 (d, $J = 7.6$ Hz, 1H, $\text{C}_7\text{-H}$), 6.46 (td, $J = 7.6, 1.2$ Hz, 1H, $\text{C}_5\text{-H}$), 6.22 (d, $J = 7.2$ Hz, 1H, $\text{C}_4\text{-H}$), 6.05 (d, $J = 8.4$ Hz, 1H, $\text{C}_7''\text{-H}$), 5.52 (d, $J = 8.0$ Hz, 1H, $\text{C}_1\text{-H}$), 4.67 (ddd, $J = 10, 8.0, 5.6$ Hz, 1H, $\text{C}_{7a'}\text{-H}$), 2.71–2.64 (m, 1H, $\text{C}_5\text{-H}$), 2.60–2.54 (m, 1H, $\text{C}_5\text{-H}$), 2.45–2.34 (m, 1H, $\text{C}_7\text{-H}_a$), 2.28–2.20 (m, 1H, $\text{C}_6\text{-H}$), 2.13–2.02 (m, 1H, $\text{C}_6\text{-H}$), 2.01–1.94 (m, 1H, $\text{C}_7\text{-H}_b$), 1.68 (s, 3H, $\text{N}_1''\text{-CH}_3$) ppm; ^{13}C NMR (DMSO d_6 , 100 MHz) δ 201.7 (q, C_{10}), 176.9 (q, C_2), 170.4 (q, C_2''), 142.1 (q, C_8''), 141.6 (q, C_8), 132.4 (q), 131.6 (q), 130.2 (q), 129.5 (q), 129.3 (CH), 129.0 (CH), 128.8 (CH), 128.0 (CH), 127.6 (q), 127.0 (q), 126.7 (CH), 126.4 (CH), 126.1 (CH), 126.0 (CH), 126.0 (q), 125.7 (CH), 125.6 (CH), 124.6 (CH), 124.3 (q), 123.1 (CH), 122.9 (2xq), 122.4 ($\text{C}_5\text{-H}$), 120.4 (C_3H), 109.4 ($\text{C}_7''\text{H}$), 109.1 (C_7H), 76.1 (C_3/C_3''), 65.9 (C_2/C_3''), 65.0 ($\text{C}_{7a'}\text{H}$), 57.2 (C_1H), 46.6 ($\text{C}_5\text{-CH}_2$), 30.8 ($\text{C}_7\text{-CH}_2$), 29.8 ($\text{C}_6\text{-CH}_2$), 24.9 ($\text{N}_1''\text{-CH-CH}_3$).

4.1.1.11. (1'S,2'R,3S,7a'S)-5,5''-dichloro-1''-methyl-1'-(1-pyrenoyl)-dispiro[indoline-3,3'-pyrrolizidine-2',3''-indoline]-2,2''-diones (**5k**) and (1'R,2'S,3S,7a'S)-5,5''-dichloro-1''-methyl-2'-(1-pyrenoyl)-dispiro[indoline-3,3'-pyrrolizidine-1',3''-indoline]-2,2''-diones (**6k**)



5k, 66%

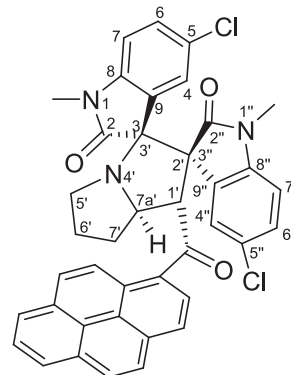


6k, 34%

Yellow crystals, mp 159–160 °C; **5k**: yield (0.364 g, 55%) from 218 mg (1.2 mmol) of **1b** and 422 mg (1.0 mmol) of **4d**. ^1H NMR (DMSO d_6 , 400 MHz) δ 10.60 (s, 1H, $\text{N}_1\text{-H}$, major), 8.35–8.03 (m, 7 H_{pyrene}), 7.92 (d, $J = 9.2$ Hz, 1 H_{pyrene}), 7.85 (d, $J = 2.4$ Hz, 1H, $\text{C}_4''\text{-H}$), 7.24 (dd, $J = 8.4, 2.0$ Hz, 1H, $\text{C}_6''\text{-H}$), 7.22 (d, $J = 9.2$ Hz, 1 H_{pyrene}), 7.01 (dd, $J = 8.4, 2.0$ Hz, 1H, $\text{C}_6\text{-H}$), 6.60 (d, $J = 8.4$ Hz, 1H, $\text{C}_7\text{-H}$), 6.16 (d, $J = 2.2$ Hz, 1H, $\text{C}_4\text{-H}$), 6.10 (d, $J = 8.4$ Hz, 1H, $\text{C}_7''\text{-H}$), 5.47 (d, $J = 8.0$ Hz, 1H, $\text{C}_1\text{-H}$), 4.69 (ddd, $J = 10, 8.0, 5.6$ Hz, 1H, $\text{C}_{7a'}\text{-H}$), 2.72 (t, 1H, $J = 8.4$ Hz, $\text{C}_5\text{-H}$), 2.44–2.34 (m, 2H, $\text{C}_5\text{-H}$ & $\text{C}_7\text{-H}_a$), 2.26–1.98 (m, 3H, $\text{C}_6\text{-CH}_2$ & $\text{C}_7\text{-H}_b$), 1.72 (s, 3H, $\text{N}_1''\text{-CH}_3$) ppm; ^{13}C NMR (DMSO d_6 , 100 MHz) δ 201.5 (q, C_{10}), 176.6 (q, C_2), 170.2 (q, C_2''), 141.6 (q, C_8''), 141.0 (q, C_8), 132.5 (q), 131.5 (q),

130.3 (q), 129.5 (q), 129.2 (CH), 129.1 (CH), 128.1 (CH), 126.8 (CH), 127.3 (q), 127.0 (q), 126.8 (CH), 126.5 (CH), 126.3 (q), 126.1 (q), 126.0 (CH), 126.0 (2CH), 125.7 (CH), 125.6 (CH), 124.8 (CH), 124.3 (q), 123.1 (CH), 122.9 (q, 2xC), 122.4 (CH), 110.5 ($\text{C}_7''\text{H}$), 109.7 (C_7H), 76.2 (C_3/C_3''), 65.9 (C_2/C_3''), 65.1 ($\text{C}_{7a'}\text{-H}$), 57.2 ($\text{C}_1\text{-H}$), 46.5 ($\text{C}_5\text{-CH}_2$), 30.8 ($\text{C}_7\text{-CH}_2$), 29.8 ($\text{C}_6\text{-CH}_2$), 25.0 ($\text{N}_1''\text{-CH}_3$). **6k**: Yield (0.188 g, 29%) from 218 mg of **1b** and 422 mg of **4d**. ^1H NMR (DMSO d_6 , 100 MHz) δ 10.78 (s, 1H, $\text{N}_1\text{-H}$), 8.30 (d, $J = 8.0$ Hz, 2 H_{pyrene}), 8.20 (d, $J = 8.8$ Hz, 1 H_{pyrene}), 8.15 (d, $J = 8.8$ Hz, 1 H_{pyrene}), 8.14 (d, $J = 1.6$ Hz, 1H, $\text{C}_4''\text{-H}$), 8.12–8.00 (m, 5 H_{pyrene}), 7.83 (d, $J = 2.4$ Hz, 1H, $\text{C}_4\text{-H}$), 7.36 (dd, $J = 8.4, 2.0$ Hz, 1H, $\text{C}_6\text{-H}$), 6.96 (d, $J = 8.4$ Hz, 1H, $\text{C}_7\text{-H}$), 5.94 (dd, $J = 8.0, 2.0$ Hz, 1H, $\text{C}_6''\text{-H}$), 5.67 (d, $J = 8.4$ Hz, 1H, $\text{C}_7''\text{-H}$), 5.61 (s, 1H, $\text{C}_2\text{-H}$, minor), 4.55 (dd, $J = 8.8, 3.6$ Hz, 1H, $\text{C}_{7a'}\text{-H}$), 3.63 (dd, $J = 8.0, 4.0$ Hz, 1H, $\text{C}_5\text{-H}$), 2.80 (s, 3H, $\text{N}_1''\text{-CH}_3$), 2.60 (t, $J = 8.0$ Hz, 1H, $\text{C}_5\text{-H}$), 1.90–1.76 (m, 2H, $\text{C}_6\text{-H}$ & $\text{C}_7\text{-H}$), 1.69–1.57 (m, 1H, $\text{C}_7\text{-H}$), 1.46–1.38 (m, 1H, $\text{C}_6\text{-H}$) ppm; ^{13}C NMR (DMSO d_6 , 100 MHz) δ 200.2 (q, C_{10}), 178.3 (q, C_2), 178.0 (q, C_2''), 142.1 (q, C_8''), 140.6 (q, C_8), 132.7 (q), 131.0 (q), 130.7 (q), 130.1 (q), 129.4 (q), 129.3 (CH), 129.0 (CH), 128.9 (q), 127.9 (CH), 127.2 (q), 126.7 (CH), 126.6 (q), 126.4 (2xCH), 126.0 (CH), 126.1 (CH), 125.9 (CH), 125.2 (CH), 125.1 (CH), 124.9 (q), 123.3 (CH), 123.0 (q), 122.7 (q), 122.2 (CH), 110.7 ($\text{C}_7''\text{H}$), 107.7 ($\text{C}_7\text{-H}$), 73.5 ($\text{C}_{7a'}\text{-H}$), 72.5 (C_3/C_3''), 67.3 ($\text{C}_2\text{-H}$), 62.1 (C_1/C_3''), 49.5 ($\text{C}_5\text{-CH}_2$), 26.1 ($\text{N}_1''\text{-CH}_3$), 25.9 ($\text{C}_7\text{-CH}_2$), 24.0 ($\text{C}_6\text{-CH}_2$).

4.1.1.12. (1'S,2'R,3S,7a'S)-5,5''-dichloro-1,1''-dimethyl-1'-(1-pyrenoyl)-dispiro[indoline-3,3'-pyrrolizidine-2',3''-indoline]-2,2''-diones (**5l**)



Yellow crystals, mp 206–208 °C; yield 0.449 g (67%) from 235 mg (1.2 mmol) of **1c** and 422 mg (1.0 mmol) of **4d**. ^1H NMR (DMSO d_6 , 400 MHz) δ 8.36–8.17 (m, 5 H_{pyrene}), 8.12–8.05 (m, 2 H_{pyrene}), 7.92 (d, $J = 9.2$ Hz, 1 H_{pyrene}), 7.86 (d, $J = 2.4$ Hz, 1H, $\text{C}_4''\text{-H}$), 7.24 (dd, $J = 8.4, 2.0$ Hz, 1H, $\text{C}_6''\text{-H}$), 7.22 (d, $J = 9.2$ Hz, 1 H_{pyrene}), 7.12 (dd, $J = 8.4, 2.0$ Hz, 1H, $\text{C}_6\text{-H}$), 6.82 (d, $J = 8.4$ Hz, 1H, $\text{C}_7\text{-H}$), 6.22 (d, $J = 2.2$ Hz, 1H, $\text{C}_4\text{-H}$), 6.06 (d, $J = 8.4$ Hz, 1H, $\text{C}_7''\text{-H}$), 5.49 (d, $J = 8.0$ Hz, 1H, $\text{C}_1\text{-H}$), 4.73 (ddd, $J = 10, 8.0, 5.6$ Hz, 1H, $\text{C}_{7a'}\text{-H}$), 3.08 (s, 3H, $\text{N}_1''\text{-CH}_3$), 2.70 (t, 1H, $J = 8.4$ Hz, $\text{C}_5\text{-H}$), 2.47–2.35 (m, 2H, $\text{C}_5\text{-H}$ & $\text{C}_7\text{-H}_a$),

2.26–2.00 (m, 3H, C₆–CH–CH₂ & C₇–H_b), 1.60 (s, 3H, N₁–CH₃) ppm; ¹³C NMR (DMSO *d*₆, 100 MHz) δ 201.5 (q, C₁₀), 175.2 (q, C₂), 170.3 (q, C_{2'}), 142.6 (q, C_{8'}), 141.8 (q, C₈), 132.8 (q, C_{pyrene}), 131.7 (q, C_{pyrene}), 130.5 (q, C_{pyrene}), 129.8 (q, C_{pyrene}), 129.5 (CH), 129.4 (2xCH), 128.4 (CH), 127.3 (q, C_{pyrene}), 127.2 (q, C_{pyrene}), 127.0 (CH), 126.8 (CH), 126.5 (q, C_{pyrene}), 126.3 (2xCH), 126.1 (CH), 126.0 (CH), 125.9 (q, C_{pyrene}), 125.4 (q, C_{pyrene}), 124.7 (CH), 123.5 (CH), 123.2 (2xCH–Cl), 122.6 (CH), 110.1 (C₇H), 109.8 (C_{7'}H), 76.2 (C₃/C_{3'}), 65.5 (C₂/C_{2'}), 65.4 (C_{7a}H), 57.4 (C₁H), 46.9 (C₅–CH₂), 31.0 (C₇–CH₂), 30.2 (C₆–CH₂), 26.1 (N₁'–CH₃), 25.2 (N₁–CH₃).

4.2. Computational details

Quantum chemical calculations were performed to obtain cycloaddition free energy profiles following a previously published protocol (Domingo, 2016). Geometry optimizations were performed in vacuum with density functional theory (DFT) using the B3LYP exchange correlation functional (Miehlich et al., 1989) and the People's double-zeta basis set (6-31G) with additional polarization function and diffuse function on the heavy atoms (B3LYP/6-31G + (d)) as implemented in Gaussian 16 software. Frequency calculations were performed with the optimized ground-state and transition-state geometries at the same level of theory. Relative energies were calculated with respect to the sum of the energies of the reactants. The energy values were converted to kcal/mol by Hartree per particle, using 627.509467 as the conversion factor.

The global electronic properties of series **3a-c** and compounds **4a-d** were estimated according to the equations of Parr and Domingo (Velikorodov et al., 2011; Domingo et al., 2002). The electronic chemical potential μ and chemical hardness η were both determined from the one-electron energies of the highest occupied molecular orbital (HOMO) and the lowest unoccupied molecular orbital (LUMO), E_{HOMO} and E_{LUMO}, as $\mu = (E_{\text{HOMO}} + E_{\text{LUMO}})/2$ and $\eta = (E_{\text{LUMO}} - E_{\text{HOMO}})$, respectively. Then, the global electrophilicity (ω) was calculated using the electronic chemical potential (μ) and chemical hardness (η) according to the formula $\omega = \mu^2/2\eta$. Then, the global nucleophilicity (N) is expressed as follows: $N = E_{\text{HOMO}} - E_{\text{HOMO(TCE)}}$, where tetracyanoethylene (TCE) was used as a reference because it provides the lowest HOMO energy of many organic molecules previously studied in polar cycloadditions.

Regional Fukui functions for electrophilic (f_k^-) and nucleophilic (f_k^+) attacks were obtained from a one-point calculation on the optimized ground state structures of the molecules, as described in the literature (Miehlich et al., 1989). The electrophilic (P_k^+) and nucleophilic (P_k^-) Parr functions were obtained by analyzing the Mulliken atomic spin densities of the radical anion and radical cation, respectively, by one-point energy calculations over the optimized neutral geometries using the unrestricted B3LYP formalism for radical species (Parr et al., 1999).

CRedit authorship contribution statement

Essam M. Hussein: Conceptualization, Methodology, Data curation, Validation, Investigation, Visualization, Project administration, Supervision, Funding acquisition, Writing –

review & editing. **Ziad Moussa:** Data curation, Validation, Funding acquisition, Visualization. **Uttam Pal:** Software, Visualization. **Reem I. Alsantali:** Data curation, Validation, Investigation, Funding acquisition. **Abdullah Y.A. Alzahrani:** Data curation, Validation, Investigation, Funding acquisition. **Rami J. Obaid:** Data curation, Validation, Investigation, Funding acquisition. **Fawaz M. Alzahrani:** Methodology, Data curation, Validation, Investigation. **Munirah M. Al-Rooqi:** Data curation, Validation, Investigation, Funding acquisition. **Meshari A. Alsharif:** Data curation, Validation, Investigation, Funding acquisition. **Nizar El Guesmi:** Validation, Data curation, Investigation. **Rabab S. Jassas:** Data curation, Validation, Investigation, Funding acquisition. **M. Shaheer Malik:** . **Hatem M. Altass:** . **Samir K. Pal:** Validation. **Tanusri Saha Dasgupta:** Validation. **Saleh A. Ahmed:** Conceptualization, Methodology, Data curation, Validation, Investigation, Visualization, Project administration, Supervision, Funding acquisition, Writing – review & editing.

Declaration of Competing Interest

The authors declare that they have no known competing financial interests or personal relationships that could have appeared to influence the work reported in this paper.

Acknowledgments

The authors extend their appreciation to the Deanship of Scientific Research at King Khalid University for funding this work through the Small Research Project under grant number (RGP.1/124/42). The authors would like to acknowledge the Deanship of Scientific Research at Umm Al-Qura University, for supporting this work by Grant code: 22UQU4350067DSR01. Also, the authors would like to extend their sincere appreciation to Taif University Researchers Supporting Project number (TURSP-2020/312), Taif University, Taif, Saudi Arabia. Dr. Ziad Moussa is grateful to the United Arab Emirates University (UAEU) of Al-Ain and to the Research Office for supporting the research developed in his laboratory (Grant no. G00003291).

Appendix A. Supplementary material

NMR spectra of the synthesized compounds; Coordinates of the optimized geometries. Supplementary data to this article can be found online at <https://doi.org/10.1016/j.arabjc.2022.103855>.

References

- Bakthadoss, M., Sivakumar, N., 2009. Novel regio- and stereoselective synthesis of functionalized 3-spiropyrrolidines and 3-spiropyrrolidines using the Baylis-Hillman adducts derived from nitroolefins. *Synlett*, 1014–1018.
- (a) G. Bifulco, P. Dambruoso, L. Gomez-Paloma, R. Riccio, Determination of relative configuration in organic compounds by NMR spectroscopy and computational methods, *Chem. Rev.* 2007, 107, 3744–3779; (b) X. Zhang, K-Z. Lu, H-W. Yan, Z-M. Feng, Y-N. Yang, J-S. Jiang, P-C. Zhang, An ingenious method for the determination of the relative and absolute configurations of compounds containing aryl-glycerol fragments by ¹H NMR spectroscopy *RSC Adv.*, 2021, 11, 8107; (c) X. Li, K.H. Hopmann,

- J. Hudecová, J. Isaksson, J. Novotná, W. Stensen, V. Andrushchenko, M. Urbanová, J-S. Svendsen, P. Bouř, K. Ruud, Determination of absolute configuration and conformation of a cyclic dipeptide by NMR and chiral spectroscopic methods, *J. Phys. Chem. A*, 2013, 117, 1721-1736; (d) Y. Takeuchi, H. Fujisawa, R. Noyori, A very reliable method for determination of absolute configuration of chiral secondary alcohols by ¹H NMR spectroscopy, *Org. Lett.*, 2004, 6, 4607-4610; (e) T. J. Wenzel, Strategies for using NMR spectroscopy to determine absolute configuration, *Tetrahedron: Asymmetry*, 2017, 28, 1212-1219. (f) Y-N. Yang, B. Han, P-F. Yang, Z-M. Feng, J-S. Jiang, P-C. Zhang, A concise approach for determining the relative configuration of H-7 and H-8 in 8,4'-oxyneolignans by ¹H NMR spectroscopy, *Org. Chem. Front.*, 2019, 6, 886-891.
- (a) Contreras, R. R.; Fuentealba, P.; Galván, M.; Pérez, P. A direct evaluation of regional Fukui functions in molecules. *Chem. Phys. Lett.* 1999, 304, 405-413. (b) Fuentealba, P.; Pérez, P.; Contreras, R. On the condensed Fukui function. *The J. Chem. Phys.* 2000, 113, 2544-2551.
- Domingo, L.R., 2016. *Molecular electron density theory: A Modern View of Reactivity in Organic Chemistry*. *Molecules* 21, 1319.
- Domingo, L.R., Aurell, M.J., Pérez, P., Contreras, R., 2002. Quantitative characterization of the local electrophilicity of organic molecules. Understanding the regioselectivity on Diels-Alder reactions. *J. Phys. Chem. A*. 106, 6871-6875.
- (a) Domingo, L. R.; Aurell, M. J.; Perez, P.; Contreras, R. Quantitative characterization of the global electrophilicity power of common diene/dienophile pairs in Diels-Alder reactions *Tetrahedron* 2002, 58, 4417-4423. (b) Pérez, P.; Domingo, L. R.; Aurell, M. J.; Contreras, R. Quantitative characterization of the global electrophilicity pattern of some reagents involved in 1,3-dipolar cycloaddition reactions *Tetrahedron* 2003, 59, 3117-3125. (c) Arroyo, P.; Picher, M. T.; Domingo, L. R. The domino reaction between 4, 6-dinitrobenzofuroxan and cyclopentadiene. Insights on the nature of the molecular mechanism *J. Mol. Struct.* 2004, 709, 45-52. (d) Arroyo, P.; Picher, M. T.; Domingo, L. R.; Terrier, F. A DFT study of the polar Diels-Alder reaction between 4-aza-6-nitrobenzofuroxan and cyclopentadiene *Tetrahedron* 2005, 61, 7359-7365.
- (a) H.A. Dondas, C.W.G. Fishwick, R. Grigg, C. Kilner, 1,3-Dipolar cycloaddition of stabilised and non-stabilised azomethine ylides derived from uracil polyoxin C (UPoC): access to nikkomycin analogues, *Tetrahedron* 2004, 60, 3473; (b) M. Poornachandran, R. Raghunathan, Synthesis of spirooxindolo/spiroindano nitro pyrrolizidines through regioselective azomethine ylide cycloaddition reaction, *Synth. Commun.*, 2007, 37, 2507; (c) M. Boruah, D. Konwar, S.D. Sharma, KF/Al₂O₃ mediated 1,3-dipolar cycloaddition of azomethine ylides: a novel and convenient procedure for the synthesis of highly substituted pyrrolidines, *Tetrahedron Lett.* 2007, 48, 4535; (d) K. Kawashima, A. Kakehi, M. Noguchi, Generation of functionalized azomethine ylides and their application to stereoselective heterocycle synthesis: an equivalent process of C-unsubstituted nitrile ylide cycloaddition reaction, *Tetrahedron* 2007, 63, 1630.
- (a) Hussein, E. M.; Abdel-Monem, M. I. Regioselective synthesis and anti-inflammatory activity of novel dispiro[pyrazolidine-4,3'-pyrrolidine-2',3''-indoline]-2'',3,5-triones *Arkivoc* 2011, 10, 85-98. (b) Hussein, E. M.; Ahmed, S. A.; El Guesmi, N.; Khairou, K. S. 1,3-Dipolar cycloaddition approach to novel dispiro[pyrazolidine-4,3'-pyrrolizidine-2',3''-indoline]-2'',3,5-triones *J. Chem. Res.* 2017, 41, 346-351. (c) Hussein, E. M.; Ahmed, S. A.; Althagafi, I. I. A convenient regioselective synthesis of novel spirooxindolinopyrrolizidines incorporating the pyrene moiety through [3 + 2]-cycloaddition reaction *Heterocycl. Commun.* 2017, 23, 379-384. (d) Hussein, E. M.; Moussa, Z.; Ahmed, S. A. Exclusive regioselective 1,3-dipolar cycloaddition of 9-diazo-9H-fluorene and diphenyldiazomethane to 2-arylideneindane-1,3-diones: new approach toward effective synthesis of novel spiroazole derivatives *Monatsh. Chem.* 2018, 149, 2021-2030. (e) Hussein, E. M.; Moussa, Z.; El Guesmi, N.; Ahmed, S. A. Facile access to regio- and stereoselective synthesis of highly functionalized spiro[indoline-3,2'-pyrrolidines] incorporating a pyrene moiety: experimental, photophysical and theoretical approach. *RSC Adv.* 2018, 8, 24116-24127. (f) Hussein, E. M.; El Guesmi, N.; Moussa, Z.; Pal, U.; Pal, S. K.; Saha-Dasgupta, T.; Ahmed, S. A. Unprecedented regio- and stereoselective synthesis of pyrene-grafted dispiro[indoline-3,2'-pyrrolidine-3,3''-indolines]: expedient experimental and theoretical insights into polar [3 + 2] cycloaddition. *ACS Omega*, 2020, 5, 24081-24094.
- Jaramillo, P., Domingo, L.R., Chamorro, E., Pérez, P., 2008. A further exploration of a nucleophilicity index based on the gas-phase ionization potentials. *J. Mol. Struct. THEOCHEM.* 865, 68-72.
- (a) P. Merino, J. Revuelta, T. Tejero, U. Chiacchio, A. Rescificinab, G. Romeoc, A DFT study on the 1,3-dipolar cycloaddition reactions of C-(methoxycarbonyl)-N-methyl nitrene with methyl acrylate and vinyl acetate, *Tetrahedron*, 2003, 59, 3581; (b) W. Benchouk, S. M. Mekelleche, M.J. Aurell, L.R. Domingo, Understanding the regio- and chemoselective polar [3 + 2] cycloaddition of the Padwa carbonyl ylides with α -methylene ketones. A DFT study, *Tetrahedron*, 2009, 65, 4644; (c) G. Bentabed-Ababsa, A. Derdour, T. Roisnel, J.A. Saez, P. Perez, E. Chamorro, L.R. Domingo, F.A. Mongin, A combined experimental and theoretical study of the polar [3+2] cycloaddition of electrophilically activated carbonyl ylides with aldehydes and imines, *J. Org. Chem.* 2009, 74, 2120; (d) A.K. Nacereddine, W. Yahia, S. Bouacha, A. Djerourou, A theoretical investigation of the regio- and stereoselectivities of the 1,3-dipolar cycloaddition of C-diethoxyphosphoryl-N-methylnitrene with substituted alkenes, *Tetrahedron Lett.* 2010, 51, 2617; (e) A. R. Suresh Babu and R. Raghunathan, Ultrasonic assisted-silica mediated [3 + 2] cycloaddition of azomethine ylides—a facile multicomponent one-pot synthesis of novel dispiroheterocycles, *Tetrahedron* 2007, 48, 6809.
- (a) Miehlich, B.; Savin, A.; Stoll, H.; Preuss, H. Results obtained with the correlation energy density functionals of Becke and Lee, Yang and Parr. *Chem. Phys. Lett.* 1989, 157, 200-206. (b) Becke, A. D. Density-functional thermochemistry. III. The role of exact exchange. *J. Chem. Phys.* 1993, 98, 5648-5652.
- (a) R.J. Monlineux, In *Alkaloids: Chemical and biological perspective*; Pelletier, S. W., Ed.; Wiley: New York, NY, 1987; Chapter 1; (b) S. Fujimori, *Jap. Pat. Appl.* 88-2912; *Chem. Abstr.* 1990, 112, 98409.
- Padwa, A., Pearson, W.H., 2002. *Synthetic Applications of 1,3 Dipolar Cycloaddition Chemistry toward Heterocycles and Natural Products*. John Wiley & Sons Inc..
- (a) Parr, R. G.; Szentpály, L.; Liu, S. Electrophilicity index. *J. Am. Chem. Soc.* 1999, 121, 1922-1924. (b) Pérez, P.; Toro-Labbé, A.; Aizman, A.; Contreras, R. Comparison between experimental and theoretical scales of electrophilicity in benzhydryl cations. *J. Org. Chem.* 2002, 4747-4752. (c) Domingo, L. R.; Chamorro, E.; Pérez, P. Understanding the reactivity of captodative ethylenes in polar cycloaddition reactions. A theoretical study. *J. Org. Chem.* 2008, 73, 4615-4624. (d) Domingo, L. R.; Pérez, P. The nucleophilicity N index in organic chemistry. *Org. Biomol. Chem.* 2011, 9, 7168-7175. (e) Chattaraj, K.; Duley, P. S.; Domingo, L. R. Understanding local electrophilicity/nucleophilicity activation through a single reactivity difference index. *Org. Biomol. Chem.* 2012, 10, 2855-2861. (f) Domingo, L. R.; Pérez, P.; Sáez, J. A. Understanding the local reactivity in polar organic reactions through electrophilic and nucleophilic Parr functions. *RSC Adv.* 2013, 3, 1486-1494. (g) Domingo, L. R.; Ríos-Gutiérrez, M.; Pérez, P. Applications of the conceptual density functional theory indices to organic chemistry reactivity. *Molecules.* 2016, 21, 748.
- (a) W.G. Rajeswaran, R.B. Labroo, E.A. Cohen, Synthesis of 5-[(indol-2-on-3-yl)methyl]-2,2-dimethyl-1,3-dioxane-4,6-diones and spirocyclopropyloxindole derivatives. Potential aldose reductase inhibitors, *J. Org. Chem.* 64 (1999) 1369; (b) J.F.M. da Silva, S.J. Garden, A.C. Pinto, *The Chemistry of Isatins: a Review from 1975*

- to 1999, *J. Braz. Chem. Soc.* 2001, 12, 273; (c) C.V. Galliford, K.V. Scheidt, Pyrrolidinyloxyindole natural products as inspirations for the development of potential therapeutic agents, *Angew. Chem. Int. Ed.* 2007, 46, 8748; (d) P. Shanmugam, B. Viswambharan, K. Selvakumar, S. Madhavan, A facile and efficient synthesis of highly functionalised 3,3'-dispiropyrrrolidine- and 3,3'-dispiropyrrrolizidine bisoxindoles via [3 + 2] cycloaddition, *Tetrahedron Lett.* 2008, 49, 2611.
- (a) M. Rios-Gutierrez, L.R. Domingo, Unravelling the mysteries of the [3 + 2] cycloaddition reactions, *Eur. J. Org. Chem.*, 2019, 267; (b) R. Jasiński, A new insight on the molecular mechanism of the reaction between (Z)-C,N-diphenylnitron and 1,2-bis(methylene-3,3,4,4,5,5-hexamethyl)cyclopentane, *J. Mol. Graphics Modell.* 2019, 94, 107461; (c) R. Jasiński, In the searching for zwitterionic intermediates on reaction paths of [3 + 2] cycloaddition reactions between 2,2,4,4-tetramethyl-3-thiocyclobutanone S-methylide and polymerizable olefins, *RSC Adv.* 2015, 5, 101045; (d) R. Jasiński, Competition between one-step and two-step mechanism in polar [3 + 2] cycloadditions of (Z)-C-(3,4,5-trimethoxyphenyl)-N-methyl-nitron with (Z)-2-EWG-1-bromo-1-nitroethenes, *Comput. Theor. Chem.* 2018, 1125, 77; (e) R. Jasiński, M. Ziółkowska, O. Demchuk, A. Maziarka, Regio- and stereoselectivity of polar [2 + 3] cycloaddition reactions between (Z)-C-(3,4,5-trimethoxyphenyl)-N-methylnitron and selected (E)-2-substituted nitroethenes, *Cent. Eur. J. Chem.* 2014, 12, 586; (f) R. Jasiński, A stepwise, zwitterionic mechanism for the 1,3-dipolar cycloaddition between (Z)-C-4-methoxyphenyl-N-phenylnitron and gem-chloronitroethene catalysed by 1-butyl-3-methylimidazolium ionic liquid cations, *Tetrahedron Lett.* 2015, 56, 532; (g) B. Braida, C. Walter, B. Engels, P. C. Hiberty, A clear correlation between the diradical character of 1,3-dipoles and their reactivity toward ethylene or acetylene, *J. Am. Chem. Soc.* 2010, 132, 7631; (h) L.R. Domingo, M. Ríos-Gutiérrez, A molecular electron density theory study of the reactivity of azomethine imine in [3 + 2] cycloaddition reactions, *Molecules*, 2017, 22, 750; (i) M. Ríos-Gutiérrez, L. Nasri, N. A. Khorief, A. Djerourou, L. R. Domingo, A molecular electron density theory study of the [3 + 2] cycloaddition reaction between an azomethine imine and electron deficient ethylenes, *J. Phys. Org. Chem.* 2018, 31, e3830; (j) D. H. Ess, K. N. Houk, Theory of 1,3-dipolar cycloadditions: distortion/interaction and frontier molecular orbital models, *J. Am. Chem. Soc.* 2008, 130, 10187–10198; (k) R. A. Firestone, The low energy of concert in many symmetry-allowed cycloadditions supports a stepwise-diradical mechanism, *Int. J. Chem. Kinet.* 2013, 45, 415–428. (l) L. R. Domingo, M. Rios-Gutierrez, P. Perez, A molecular electron density theory study of the role of the copper metalation of azomethine ylides in [3 + 2] cycloaddition reactions, *J. Org. Chem.* 2018, 83, 2182–219(m) A. S. Novikov; M. L. Kuznetsov. Theoretical study of Re(IV) and Ru(II) bis-isocyanide complexes and their reactivity in cycloaddition reactions with nitrones, *Inorg. Chim. Acta*, 2012, 380, 78-89. (n) A.S. Novikov; M.L. Kuznetsov; A.J.L. Pombeiro. Theory of the formation and decomposition of n-heterocyclic aminoxy-carbenes through metal-assisted [2 + 3]-dipolar cycloaddition/retro-cycloaddition. *Chem. Eur. J.*, 2013, 19, 2874-2888. (o) M.A. Kinzhalov, A. S. Novikov, K.V. Luzyanin, M. Haukka, A.J. Pombeiro, V.Y. Kukushkin. Pd II-mediated integration of isocyanides and azide ions might proceed via formal 1, 3-dipolar cycloaddition between RNC ligands and uncomplexed azide. *New J. Chem.* 2016, 19, 521-52(p) M.A. Kinzhlov, A.S. Legkodukh, T.B. Anisimova, A.S. Novikov, V.V. Suslonov, K.V. Luzyanin, V.Y. Kukushkin. Tetrazol-5-ylidene gold (III) complexes from sequential [2 + 3] cycloaddition of azide to metal-bound Isocyanides and N4 alkylation. *Organometallics* 2017, 36, 3974-3980. (q) A. A. Melekhova, A. S. Smirnov, A. S. Novikov, T. L. Panikorovskii, N. A. Bokach, V. Y. Kukushkin. Copper(I)-catalyzed 1,3-dipolar cycloaddition of ketonitrones to dialkylcyanamides: a step toward sustainable generation of 2,3-dihydro-1,2,4-oxadiazoles, *ACS Omega* 2017, 2, 1380-1391. (r) A.Y. Dubovtsev, V.V. Zvereva, N.V. Shcherbakov, D.V. Dar'in, A.S. Novikov, V.Y. Kukushkin. Acid-catalyzed [2 + 2] cycloaddition of two cyanamides and one ynamide: highly regioselective synthesis of 2, 4, 6-triaminopyrimidines. *Org. Biomol. Chem.* 2021, 19, 4577-4584. (s) E.V. Sirotkina, M.M. Efremova, A.S. Novikov, V.V. Zarubaev, I.R. Orshanskaya, G.L. Starova, R.R. Kostikov, A.P. Molchanov. Regio- and diastereoselectivity of the cycloaddition of aldonitrones with benzyldienecyclopropane: An experimental and theoretical study. *Tetrahedron.* 2017, 73, 3025-3030. (t) M.M. Efremova, A.S. Novikov, R.R. Kostikov, T.L. Panikorovsky, A.V. Ivanov, A.P. Molchanov. Regio- and diastereoselectivity of the cycloaddition of nitrones with N-propadienyloxyindole and pyrroles. *Tetrahedron.* 2018, 74, 174-183. (u) Dmitriev VA, Efremova MM, Novikov AS, Zarubaev VV, Slita AV, Galochkina AV, Starova GL, Ivanov AV, Molchanov AP. Highly efficient and stereoselective cycloaddition of nitrones to indolyl- and pyrrolylacrylates. *Tetrahedron Lett.* 2018, 59, 2327-2331. Teterina PS, Efremova MM, Sirotkina EV, Novikov AS, Khoroshilova OV, Molchanov AP. A highly efficient and stereoselective cycloaddition of nitrones to N-arylitacetonimides. *Tetrahedron Lett.* 2019, 60, 151063. (v) Efremova MM, Molchanov AP, Novikov AS, Starova GL, Muryleva AA, Slita AV, Zarubaev VV. 1, 3-Dipolar cycloaddition of N-allyl substituted polycyclic derivatives of isoindole-1, 3-dione with nitrones and nitrile oxides: An experimental and theoretical investigation. *Tetrahedron.* 2020, 76, 131104. (w) Efremova MM, Makarova AA, Novikov AS, Kryukova MA, Kuznetsov MA, Molchanov AP. Regio- and stereoselective (3 + 2)-cycloaddition reactions of nitrones with cyclic allenes. *Org. Biomol. Chem.* 2021, 19, 9773-9784. (x) Chen HX, Zhang Y, Zhang Y, He X, Zhang ZW, Liang H, He W, Jiang X, Chen X, Qiu L. Synthesis of six-membered spirooxindoles via a chiral Bronsted acid-catalyzed asymmetric intramolecular Friedel-Crafts reaction. *RSC advances.* 2018, 8, 37035-37039. (y) Liang H, He X, Zhang Y, Chen B, Ouyang JS, Li Y, Pan B, Reddy CV, Chan WT, Qiu L. Copper-catalyzed (4 + 1) and (3 + 2) cyclizations of iodonium ylides with alkynes. *Chem. Commun.* 2020, 56, 11429-114232.
- Serov, A.B., Kartsev, V.G., Aleksandrov, Y.A., Dolgushinc, F.M., 2005. 1,3-Dipolar cycloaddition reaction of heteroaromatic N-ylides with 3-[(E)-2-aryl(hetaryl)-2-oxoethylidene]indolin-2-ones. *Russ. Chem. Bull.* 54, 2432–2436.
- Velikorodov, A.V., Poddubnyi, O.Y., Krivosheev, O.O., Titova, O.L., 2011. Three-component synthesis of spiro compounds with a carbamate functionality. *Russ. J. Org. Chem.* 47, 402–404.
- Velikorodov, A.V., Ionova, V.A., Degtyarev, O.V., Sukhenko, L.T., 2013. Synthesis and Antimicrobial and Antifungal Activity of Carbamate-Functionized Spiro Compounds. *Pharm. Chem. J.* 46, 715–719.
- Weng, J., Mei, Q., Ling, Q.Q., Fan, Q., Huang, W., 2012. A new colorimetric and fluorescent ratiometric sensor for Hg²⁺ based on 4-pyren-1-yl-pyrimidine. *Tetrahedron* 68, 3129.
- (a) Yan, X.-X.; Peng, Q.; Zhang, Y.; Zhang, K.; Hong, W.; Hou, X.-L.; Wu, Y.-D. A highly enantio- and diastereoselective Cu-catalyzed 1,3-dipolar cycloaddition of azomethine ylides with nitroalkenes *Angew. Chem. Int. Ed.* 2006, 45, 1979-1983. (b) Li, W.; Shi, M. Bronsted acid TfOH-mediated [3 + 2] cycloaddition reactions of diarylvinyldienecyclopropanes with nitriles *J. Org. Chem.* 2008, 73, 4151-4154. (c) Tsubogo, T.; Saito, S.; Seki, K.; Yamashita, Y.; Kobayashi, S. Development of catalytic asymmetric 1, 4-addition and [3 + 2] cycloaddition reactions using chiral calcium complexes *J. Am. Chem. Soc.* 2008, 130, 13321-13332. (d) Ghandi, M.; Yari, A.; Rezaei, S. J. T.; Taheri, A. Synthesis of novel spiropyrrolidine/pyrrolizine-oxindole scaffolds through 1,3-dipolar cycloadditions *Tetrahedron Lett.* 2009, 50, 4724-4726. (e) Yamashita, Y.; Guo, X.-X.; Takashita, R.; Kobayashi, S. Chiral silver amide-catalyzed enantioselective [3 + 2] cycloaddition of α -aminophosphonates with olefins *J. Am. Chem. Soc.* 2010, 132, 3262-3263.